# Interlayer bonding has bulk-material strength in extrusion additive manufacturing: new understanding of anisotropy

James Allum, Amirpasha Moetazedian, Andrew Gleadall* and Vadim V. Silberschmidt

Wolfson School of Mechanical, Electrical and Manufacturing Engineering, Loughborough University, Loughborough, LE11 3TU, UK

* Corresponding author - Tel.: +44(0) 1509 227578; E-mail: a.gleadall@lboro.ac.uk

Author preprint - final article available at: https://doi.org/10.1016/j.addma.2020.101297

## Terminology

*Aspect ratio:* The ratio of extruded-filament width to layer height.
*Extruded filament*: The deposited filament, from which the 3d printed specimens are comprised (sometimes referred to as *rasters*, *fibres*, *roads*, *tracks* or *extrudates* in other studies).
*Extruded-filament geometry*: The cross-sectional geometry of the extruded filament.
*EFW*: Extruded-filament width
*F*: Filament direction (sometimes referred to as *longitudinal direction* in other studies - parallel to the print bed)
*Interface*: The region of joining between two extruded filaments.
*Interlayer bonding:* The interfacial bonding between layers (extruded filaments).
*LH:* Layer height
*Load-bearing area*: The cross-sectional area of the specimen, which bears mechanical load.
*Specific load-bearing capacity*: The maximum load capacity of specimens normalised by the weight of the unit length of the specimen gauge.
*Z*: Z-direction (normal-to-filament direction and normal to the print bed).
*MEAM*: Material Extrusion Additive Manufacturing.

**Abstract**

This study demonstrates that the interface between layers in 3D-printed polylactide has strength of the bulk filament. Specially designed 3D-printed tensile specimens were developed to test mechanical properties in the direction of the extruded filament (F specimens), representing bulk material properties, and normal to the interface between 3D-printed layers (Z specimens). A wide range of cross-sectional aspect ratios for extruded-filament geometries were considered by printing with five different LHs and five different EFWs. Both F and Z specimens demonstrated bulk material strength. In contrast, strain-at-fracture, specific load-bearing capacity, and toughness were found to be lower in Z specimens due to the presence of filament-scale geometric features (grooves between extruded filaments). The different trends for strength as compared to other mechanical properties were evaluated with finite-element analysis. It was found that anisotropy was caused by the extruded-filament geometry and localised strain (as opposed to assumed incomplete bonding of the polymer across the interlayer interface). Additionally, effects of variation in print speed and layer time were studied and found to have no influence on interlayer bond strength. The relevance of the results to other materials, toolpath design, industrial applications, and future research is discussed. The potential to use this new understanding to interpret historic and future research studies is also demonstrated.

**Keywords**

Additive manufacturing;

Material extrusion;

Interface;

Bond strength;

Mechanical properties

## 1 Introduction and aims

Material extrusion additive manufacturing (MEAM) has played a critical role in the development and propagation of digital manufacturing in recent years. MEAM has

been technologically and socially empowering; its affordability provided digital manufacturing capabilities to a broad and diverse community of manufacturers, resulting in rapid technological development. MEAM secured investment from some of the world's most renowned manufacturers, who took advantage of the technology to reduce manufacturing costs and generate parts, which previously were impossible or prohibitively complex to manufacture with traditional methods. Examples of products manufactured using MEAM include patient specific implants and surgical guides [1,2].

MEAM for polymeric material operates by the extrusion of a polymer filament through a heated nozzle. Material is deposited in molten form onto a build plate, where it solidifies rapidly. The movement of the nozzle through X and Y axes (in the plane parallel to the print platform) results in the formation of a thin slice of the overall structure, while incremental movement in the Z direction allows a layer-by-layer build. The produced part comprises a physical embodiment of the nozzle's toolpath, manufactured in numerous layers with the appearance of being stacked in micro-slices. This layer-wise strategy gives rise to the biggest mechanical limitation of MEAM: mechanical anisotropy, and, more specifically, weakness in the direction normal to the print platform (Z direction) [3–12].

Numerous studies sought to understand and overcome the limitations of interlayer bond weakness and associated anisotropy. Broadly, there exist two areas of investigation with regard to analysis of limitations in MEAM: material and geometric factors. A number of works studied the impact of bond healing on the interface with respect to thermal factors, such as extrusion temperatures [12–16], reporting that higher nozzle temperature had the impact of increasing mechanical performance of the interface due to improved bond healing. But there are contradictions regarding the effect of nozzle feedrate (speed), with some studies finding improved strength at lower speeds [17–19], and others observing the opposite trend [20][21].

The research into geometrical factors assessed the role of LH, with some studies indicating that a reduced LH resulted in improved strength [12–15,22–24]; others disputed this, reporting the opposite trend [3,5,20]. A small number of works considered EFW (sometimes referred to as *raster width* or equivalent terms such as

*fibre*, *road*, *track* or *extrudate*); one study concluded that minimising EFW improved tensile strength [22] but the opposite trend was reported in [12].

The disagreements in these findings in part have arose as a result of variability in methodologies since there are no specific standards for mechanical testing of MEAM parts. Most studies have utilised and adapted polymer-testing standards such as ASTM D3039 [3,7,13], ASTM D638 [4,5,8,10,11,17,18,22,24], ASTM D1708 [12] and ISO 527 [6]. A further complication was the use of differing geometrical strategies (raster patterns) in different studies. Hence it is difficult to compare studies or to identify, which parameter modifications predominantly influenced test outcomes.

One study [12] was able to overcome limitations relating to geometrical complexity by utilising a test specimen geometry comprising individual extruded filaments. In their study of MEAM ABS specimens, Coogan and Kazmer observed the most significant improvement in interfacial bond strength as EFW was increased and LH was reduced. Ultimately, this study concluded that a combination of higher nozzle temperatures and reduced LH promoted increased interface temperature and pressure, resulting in enhanced bond strength thanks to greater polymer-chain diffusion. The findings by Coogan and Kazmer [12] were for the graft copolymer ABS. But it is widely recognised that linear polymer chains can interdiffuse more readily than those of ABS, and, therefore, the findings from their study may not translate to linear polymers such as polylactide (PLA), polyamide, polycarbonate and many other widely used 3D printing polymers. While mechanical anisotropy was often observed in experiments, theoretical investigations showed that reptation time was sufficient (within the time to reach below the glass transition temperature) to enable interdiffusion of polymer chains across the interface between extruded filaments, and, thus, a bulk-strength interface is feasible [25]. A study by the present authors found that surface features had a critical effect on fracture loads and identified that bond and bulk material might have similar fracture behaviours [26].

The present study is the first analysis of the effect of EFW, LH and aspect ratio of MEAM at the scale of individual extruded filaments for a linear polymer. This study focuses on the mechanical performance in both the direction of extruded filaments and of the interface between layers, using a newly developed single-filament-wide test specimen design with a wide range of extruded-filament geometries. The term

“extruded-filament width” (EFW) rather than “raster width” is used as this study considers specimens comprised of individual extruded filaments rather than raster patterns. Finite-element analysis (FEA) is employed to support thorough evaluation of experimental results. This research provides a new understanding of the effect of filament-scale geometry on mechanical performance of 3D-printed polymers, which was not developed in any previous study. This understanding is used for a new interpretation of existing experimental studies.

## 2 Methods and materials

This section outlines the materials and processes used to manufacture, measure and mechanically characterise test specimens.

### 2.1 Additive manufacturing process

Specimens for this study were manufactured using natural PLA (3DXTECH® branded NatureWorks® polylactide 4043D, Sigma Aldrich) with a density of 1.25 g / mm using a RepRap X400 3D-printing system. All specimens were produced as four-sided hollow boxes comprising single-filament walls using custom GCode generated (with in-house developed software) to enable explicit control of nozzle position, extrusion volume, speed and sequence of deposition (Fig. 1). As a result, it was possible to design tensile-testing specimens at the scale of individually extruded filaments by tailoring the volume of extrusion along the toolpath (Fig. 2) to ensure their fracture in the gauge region during loading and with overall dimensions conforming to ASTM D1708 [27]. This specimen design was successfully utilised by the authors in another study [28].

Specimens were produced with

- five variations in LH (all with a constant EFW);
- five variations of EFW (all with a constant LH)

as detailed in Table 1.

All specimens were generated to test in the direction of extruded filaments (F direction) and in the direction normal to the interlayer interface (Z direction) as show in Fig. 2 (a)

and (b), respectively. This enabled direct comparison of anisotropic mechanical performance with the same filament geometries and same toolpath (Table 1). The dimensions of all manufactured hollow boxes were 45 mm (H) x 45 mm (W). Their wall thickness was defined by the studied EFW geometry (Table 1). A nozzle with a 0.4 mm bore was utilised, heated to 210°C with a feedrate (travel speed) of 1000 mm $min^{-1}$; the platform was heated to 60°C. The advantages of utilising custom GCode as opposed to that generated using slicing software was a possibility to utilise a constant print speed and symmetrical deposition sequence to ensure the constant relative cooling time between any two points along the toolpath (Fig. 1). This reduced significantly the potential for uncontrolled thermal variability between different regions of the geometry that often occurs when using slicing software with multiple printing toolpath strategies. Therefore, all specimens were thermodynamically similar (although necessarily had considerably different cross-sectional areas), eliminating the risk of variation in bond healing due to uncontrolled thermal changes and allowing for rigorous investigation of desired parameters without unavoidable variation of other printing parameters. The GCode for the reference specimens F-0.2-0.5 and Z-0.2-0.5 of this study is available as supplementary data (for a reference purpose only; they should not be used on other 3D printers as the GCode is machine-dependent).

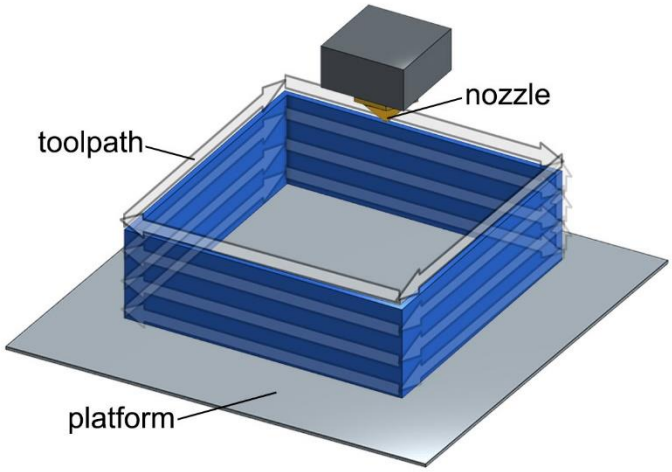


***Fig. 1*** *Toolpath strategy for generating geometries for specimen preparation.*

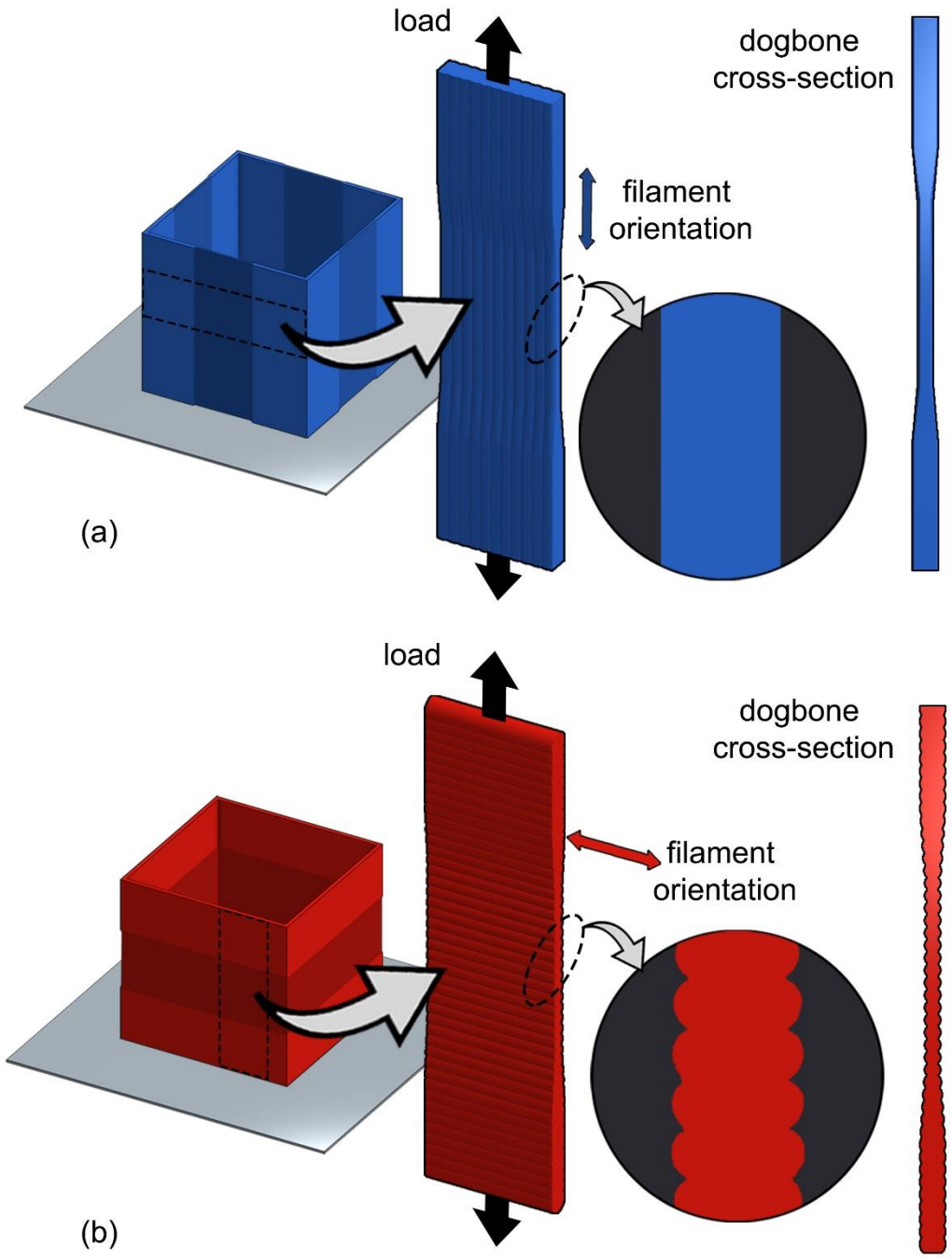


***Fig. 2*** *Two specimen types - filament direction (a) and Z direction (b) - cut from their respective 3D-printed boxes (Fig. 1) and difference in their resulting filament orientation. Dashed lines denote the cutting contours of test specimens. The cross-section of the individual filament dogbone geometry for the two specimen types is also shown.*

## 2.2 Specimen geometry and preparation

As demonstrated in Table 1, to analyse the impact of LH and EFW, and, therefore, aspect ratio, specimens were manufactured with EFWs in their gauge areas ranging from 0.4 mm to 0.6 mm (with increments of 0.05 mm), for a constant filament LH of 0.2 mm in both F (Fig. 3 (a) and (b)) and Z (Fig. 3 (c) and (d)) direction. Specimens were also produced with LH ranging from 0.1 mm to 0.3 mm (in 0.05 mm increments), for a constant EFW of 0.5 mm in both F direction (Fig. 3 (a) and (b)) and Z direction (Fig. 3 (c) and (d)). Microscopy in Fig. 3 (a) and (b) show the cross-sectional views (indicated by the hatched line in the schematic) of the F and Z specimens, respectively. The F specimens demonstrate numerous extruded filaments (Fig. 3 (a)) as they are oriented in the direction of loading (Fig. 3 (a)), whereas only the rectangular outline of the single top extruded filament can be seen in the Z specimens (Fig. 3 (b)) as the filaments are aligned normal to loading direction. The specimens with a LH of 0.2 mm and EFW of 0.5 mm are the reference specimens for both types. EFW and LH refer to the filament dimensions within the gauge section of tensile test specimen manufactured. The shoulder section was manufactured with extruded filaments that were approximately 50% wider than those in the gauge area. The aspect ratio (EFW / LH) was employed to provide an understanding of the relationship between EFW and LH; Table 1 demonstrates the aspect ratios analysed in this study for all combinations of LH and EFW. The aspect ratio ranged from 1.6, for relatively tall and narrow filaments, to 5, for relatively wide and short ones. Additionally, in order to achieve an aspect ratio of 4, which was in the range for nine designs, specimens were produced with a LH of 0.15 mm and EFW of 0.6 mm; this LH and EFW combination was selected as it was similar to the reference specimen. All specimen types were manufactured in Z and F orientations, with the only difference being the direction of the dogbone geometry relative to the deposited filaments (Fig. 2). To achieve the variation in filament geometry, two hollow four-sided boxes was produced using custom GCode programmed for each specimen type (one in Z orientation and one in F). Specimens for mechanical tests were produced by cutting the boxes as follows:

(i) boxes were cut at the corners with a razor blade mounted in a specially designed tool, to yield four walls;

(ii) the four walls were individually mounted into a second specifically designed tool comprising an array of three razor blades, as shown in **Error! Reference source not found.**;

(iii) the blades were compressed into the walls using a hydraulic press to cut with even and controlled pressure to yield two specimens per wall (**Error! Reference source not found.**).

Each F and Z specimen had dimensions of 45 mm (H) x 15 mm (W) (Fig. 3). In this study, 160 specimens were produced to investigate twenty specimen variations (ten different geometry designs, each manufactured in F and Z orientations). Eight specimens of each type were thus generated, with six of each type utilised for mechanical characterisation (two spare). At all stages of processing and testing, specimens were stored in sealed bags with silica gel desiccant to reduce the risk of water adsorption. Acronyms were utilised to denote specimens in this study, with the following naming method: “print direction”-“LH”-“EFW”. For instance, to refer to an F direction specimen with a 0.2 mm LH and a 0.5 mm EFW was denoted “F-0.2-0.5”. Table 1 gives notation for F specimens, when referring to Z specimens ‘F’ is replaced with ‘Z’.

| | | | | | | |
|---|---|---|---|---|---|---|
| **EFW (mm)** | **0.6** | | 4 (F-0.15-0.6) | 3 (F-0.2-0.6) | | |
| | **0.55** | | | 2.75 (F-0.2-0.55) | | |
| | **0.5** | 5 (F-0.1-0.5) | 3.33 (F-0.15-0.5) | **2.5 (F-0.2-0.5)** | 2 (F-0.25-0.5) | 1.6 (F-0.3-0.5) |
| | **0.45** | | | 2.25 (F-0.2-0.45) | | |
| | **0.4** | | | 2 (F-0.2-0.4) | | |
| | | **0.1** | **0.15** | **0.2** | **0.25** | **0.3** |
| | | **LH (mm)** | | | | |

**Table 1** *Aspect ratios of extruded filaments and notation (in brackets) of tested specimens. Both Z and F specimens were produced and tested (for Z specimens – replace "F" with "Z"). The reference specimen is highlighted.*

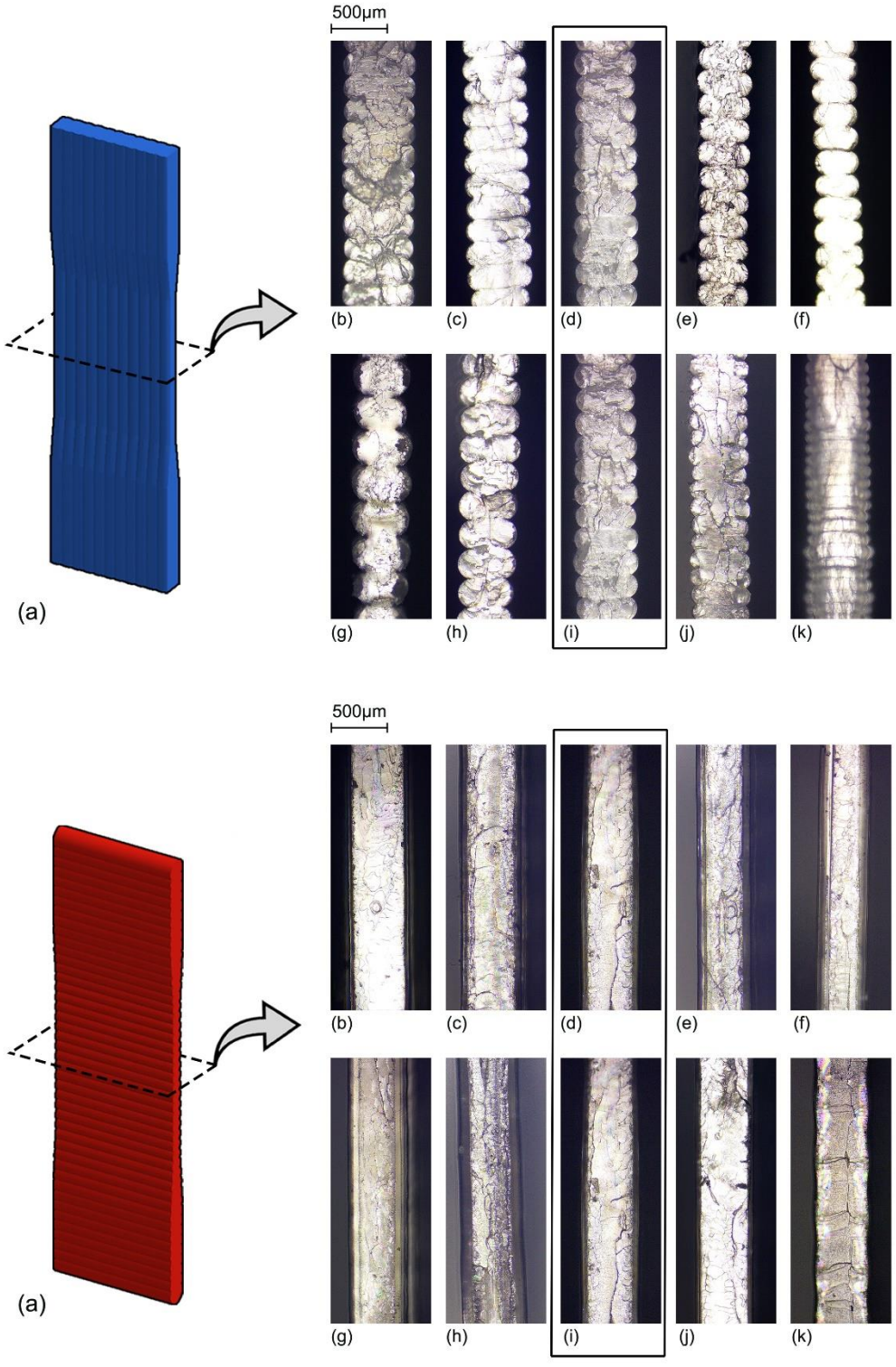


***Fig. 3*** *Cross-sectional microscopy of F (a) and Z (c) specimens in the gauge region (illustrated by a hatched line). (b) and (d) show the microscopic variation in extruded filament geometries for changing width (top rows) and height (bottom rows) along with specimen notation; the reference geometry appears twice.*

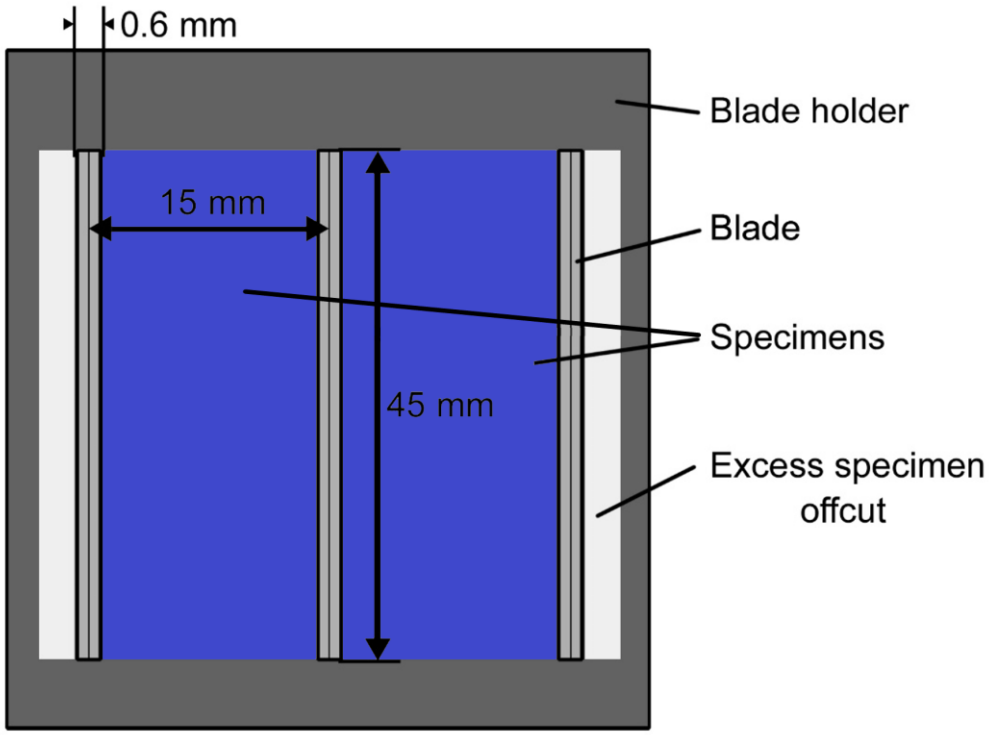


***Fig. 4*** *Schematic of the tool used to cut two specimens (in blue) from each of the walls of the manufactured boxes. Resultant cut specimens and dimensions are indicated.*

### 2.3 Mechanical characterisation

Specimens were tested in tension using an Instron 5944 system. The loading was displacement controlled at 0.5 mm $min^{-1}$, a 2 kN load cell was utilised with a specimen gauge length of 20 mm ($4.2x10^{-4}$ $s^{-1}$ strain rate). The cross-sectional area of each specimen was measured using a Zeiss Primotech optical microscope with a 5x magnification lens in conjunction with ImageJ measuring software. For each specimen, seven measurements of the bonding area of the specimen were taken, and a mean value was calculated. In addition, bond angles were measured in all Z specimen types. For this, a Zeiss Primotech optical microscope with 5x magnification lens was used in conjunction with ImageJ to collect 25 measurements for each specimen type, from which a mean value was derived. Strength (the ability to withstand load) was calculated by dividing the maximum measured load with the surface area in the region of fracture in both F and Z specimens. Specific load-bearing capacity was defined as the maximum load of specimen normalised by the weight of the unit length of the specimen gauge. This was calculated by weighing a section from

the gauge of an untested specimen of each type. This section was measured using a digital caliper. Toughness (the ability of the specimens to absorb energy before fracture) was calculated by measuring the total area underneath stress-strain curves.

## 3 Results and discussion

The results and discussion are divided into four sections:

- 3.1 - Bulk-strength interface bond, which deals with the strength of F and Z specimens with a focus on the mechanical performance of the interface (Z) compared to that of the extruded filament (F);
- 3.2 - Strain-at-fracture and toughness, which follows Section 3.1 to consider these properties and uses FEA to help analyse the experimental results;
- 3.3 - Specific load-bearing capacity, which discusses the role of filament-scale geometric features on load-bearing capacity;
- 3.4 - Applicability of results, which identifies new understanding of the results in Sections 3.1 to 3.3 using Ashby plots and applying the findings to other studies, and relevance to future research/development.

### 3.1 Bulk-strength interface bond

To understand the performance of the interface bond compared to that of bulk filament in MEAM-generated PLA specimens, this section compares the strength of F and Z specimens with varying filament geometries (LH, EFW and aspect ratio).

*LH*

Varying the LH in F and Z specimens had little impact on strength of the extruded filament (F specimens) or interface bond (Z specimens) (Fig. 5 (a)). In F specimens, mean strength was in a range from 60.6 to 68.7 MPa across different LHs, while Z specimens demonstrated a range from 54.6 to 65.6 MPa. The combined mean value of all F LH specimens was 63.9 MPa, while that for Z LH variation specimens was 59.1 MPa, a difference of just 4.8 MPa (less than the individual experimental error bars for all ten specimen groups). For one case (Z-0.2-0.5), Z specimens actually showed

greater strength than equivalent F specimens (Fig. 5 (a)), Also, the error bars overlap in most cases, highlighting the similarity of F and Z strength. In both orientations, mean maximum strengths obtained were comparable to that of bulk PLA, which was demonstrated to be between 52.5 and 80 MPa in a number of existing studies [13,29–35]. The overall similarity in performance of Z and F specimens strongly supports the hypothesis that interface strength is similar to bulk-material strength. This lends support that the material properties in the two differing orientations are very similar and that the presence of interface bond in Z specimens does not cause any substantial reduction in material performance.

*EFW*

Varying the EFWs of specimens also had a limited impact on strength of both F and Z specimens (Fig. 5 (b)), with all mean strength values falling within, or very close to, the range of mechanical performance identified for bulk PLA (52.5 and 80 MPa) [13,29–35]. Mean strength of F specimens ranged from 59.9 to 66 MPa, while Z specimens had a range from 51.2 to 67.8 MPa. Combined mean values for F was 62.6 MPa, compared to 59.4 MPa for the combined mean of Z specimens, a difference of just 5.3%, much lower than the experimental range measured for most individual specimen groups. Although F specimens achieved the highest strength in three cases (Fig. 5 (b)), in two cases, 0.2-0.5 and 0.2-0.6, Z specimens demonstrated higher strength than F ones, again supporting the theory that both F and Z specimens are capable of achieving bulk-material properties.

The cause of the larger range (and lower mean strength) in Z specimens is due to a reduced performance of Z-0.2-0.4 specimens. It is considered that this poor performance resulted from their narrowest extruded filaments, close to the lower limit of acceptable printing conditions (some specimens in this group achieved bulk strength while others did not). This hypothesis originates from the authors experience in preliminary trials (unpublished data) that the printing process experiences problems, such as discontinuous extrusion, for excessively narrow extruded filaments (e.g. 0.3 mm wide). The variability observed in Z specimens (but not F specimens) can be attributed to the sensitivity of the geometry tested in the Z orientation. Whereas performance of F specimens is the result of the combined mechanical strength of all

extruded filaments arranged side-by-side and loaded along their length, the Z direction specimens rely on the performance of every single extruded filament, and its interfacial bond with its adjacent extruded filaments. Therefore, geometrical variability occurring during the printing process had a more noticeable impact on Z specimens, as only one weakness is sufficient to induce reduced mechanical performance.

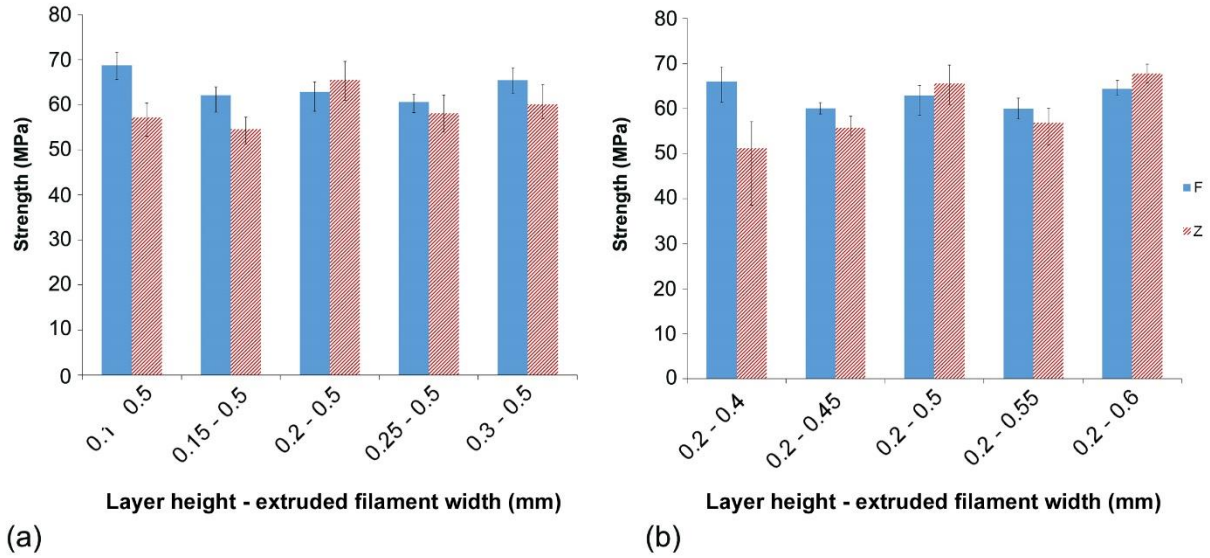


***Fig. 5*** *(a) Strength of F and Z specimens as LH is increased from 0.1 to 0.3 mm (EFW is constant at 0.5 mm). (b) Strength of F and Z specimens as EFW is increased from 0.4 to 0.6 mm (LH is constant at 0.2 mm). Error bars indicate the range of strength values for six specimens. Strength is similar for F and Z specimens, indicating that the interlayer bonds may have bulk material strength for a wide range of extruded filament geometries.*

*Aspect ratio*

To analyse the effect of aspect ratio on mechanical performance, strength was plotted against aspect ratio for all individual F and Z specimens in Fig. 6. All specimen types, irrespective of aspect ratio had rather similar strengths. Z specimens demonstrated comparable values for strength to those observed in F specimens (marginally weaker on average, but sometimes stronger than F specimens). Overall, the aspect ratio had a limited effect on strength, with specimens at all aspect ratios in both orientations showing significant similarity to bulk PLA properties [13,29–35]. The two outlying low data points for the Z specimen with an aspect ratio of 2, may be considered anomalous

if the printing process was approaching the limit of reliable extrusion for this specimen type (which had the narrowest EFW), as discussed in the previous section.

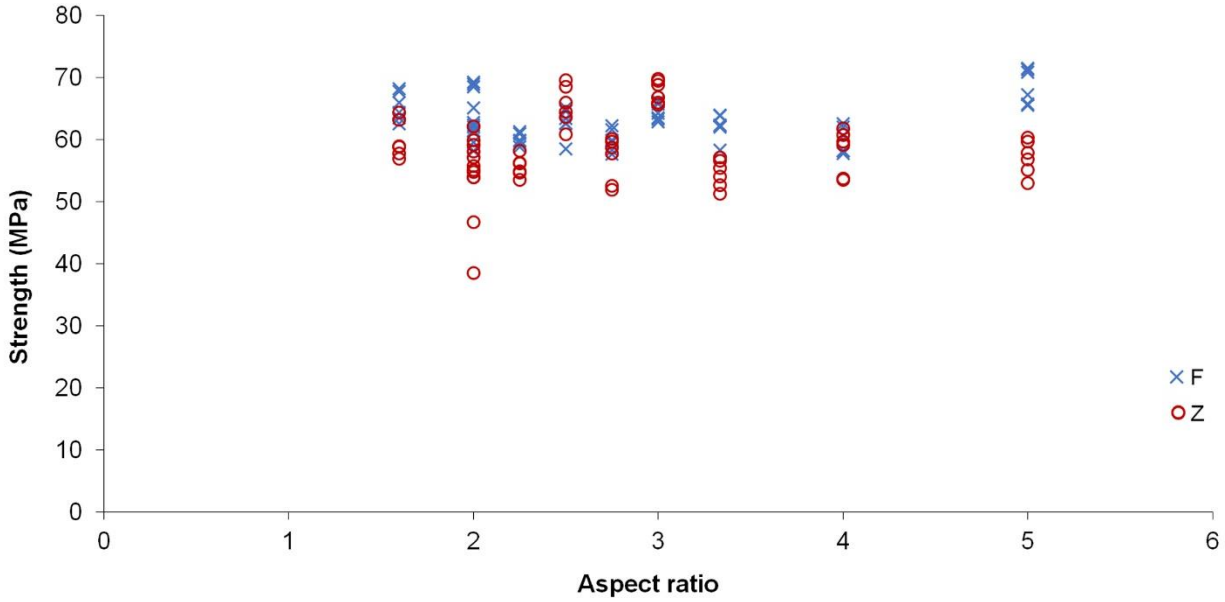


**Fig. 6** Effect of *aspect ratio (EFW / LH) on strength of F and Z specimens. F and Z specimens have similar strengths and do not show a dependency on aspect ratio.*

*Load-at-fracture vs fracture surface area*

In both F and Z specimens, the growing surface area was found to increase the load-bearing capacity (maximum load during tensile tests). Analysis of the link between the mean load-bearing capacity (mean of six replicates for each of the twenty specimens) and the mean surface area derived from microscopic measurement (Fig. 7) showed that the surface area, over which fracture occurs, was the governing factor for load-bearing capacity. Generally, Z specimens were found to have smaller surface areas than F specimens due to their geometrical narrowing at the region of interface, which will be further investigated in Section 3.3. Irrespective of the orientation of the tested specimens the location of fracture - at the interface (in the case of Z specimens) or directly through multiple extruded filaments (F specimens) - specimens with similar surface area values were able to sustain comparable loads. For example, Fig. 7 (b) and (c) show that F-0.2-0.45 and Z-0.2-0.55 have close fracture surface areas (6.37

and 6.57 $mm^2$, respectively) and similar load-bearing capacities (382 and 373 N, respectively). A linear relationship between the surface area and the load-bearing capacity was established irrespective of the specimen orientation. This is further evidence that both F and Z specimens have similar (bulk-level) material properties as demonstrated in the previous sections.

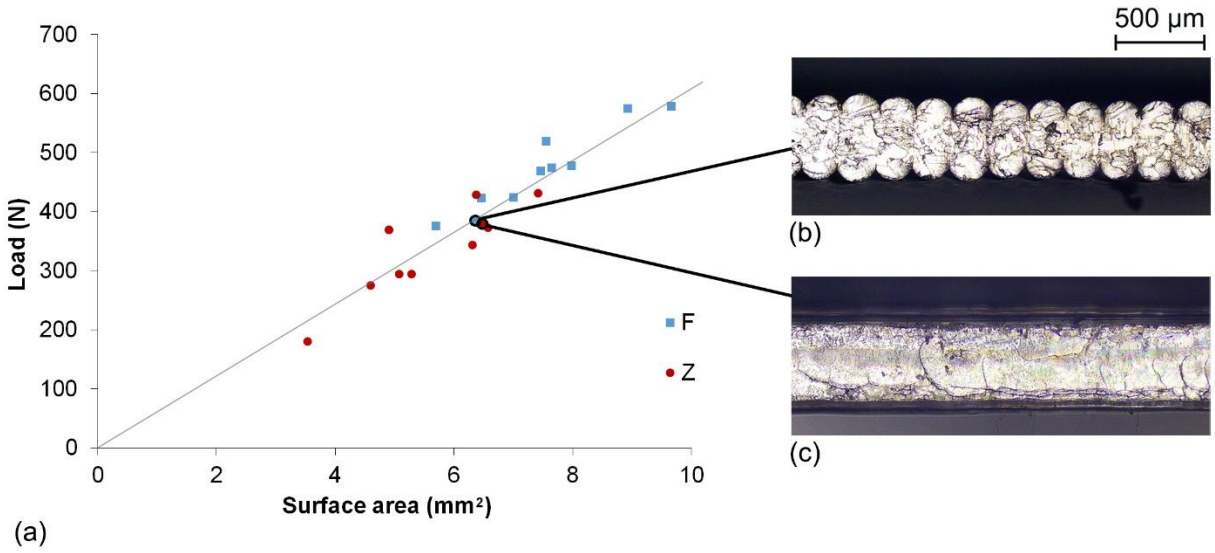


**Fig. 7** *Mean load-bearing capacity plotted against mean surface area for each specimen type in both F and Z direction. The inset microscopy of F-0.2-0.45 (b) and Z-0.2-0.55 (c) that had close fracture surface areas and equivalent load-bearing capacity even though they were tested in different orientations and had different geometric designs.*

*Stress-strain*

The stress-strain curves (Fig. 8) demonstrates tensile behaviours of one specimen of each orientation (F and Z) taken from the reference geometry 0.2 mm - 0.5 mm. Apparently both specimens achieved very similar ultimate tensile stress (UTS) (approx. 64 MPa), and the characteristics of both curves up to the yield point (at a strain of approximately 0.03) also indicates that the stiffness of F and Z specimens were very similar. Although both specimens reached similar UTS (bulk strength), the Z specimens demonstrated sudden failure shortly after UTS, whereas F specimens

demonstrated a characteristic plasticity, common for bulk PLA. The differences in strain characteristics and plasticity will be assessed in Section 3.2.

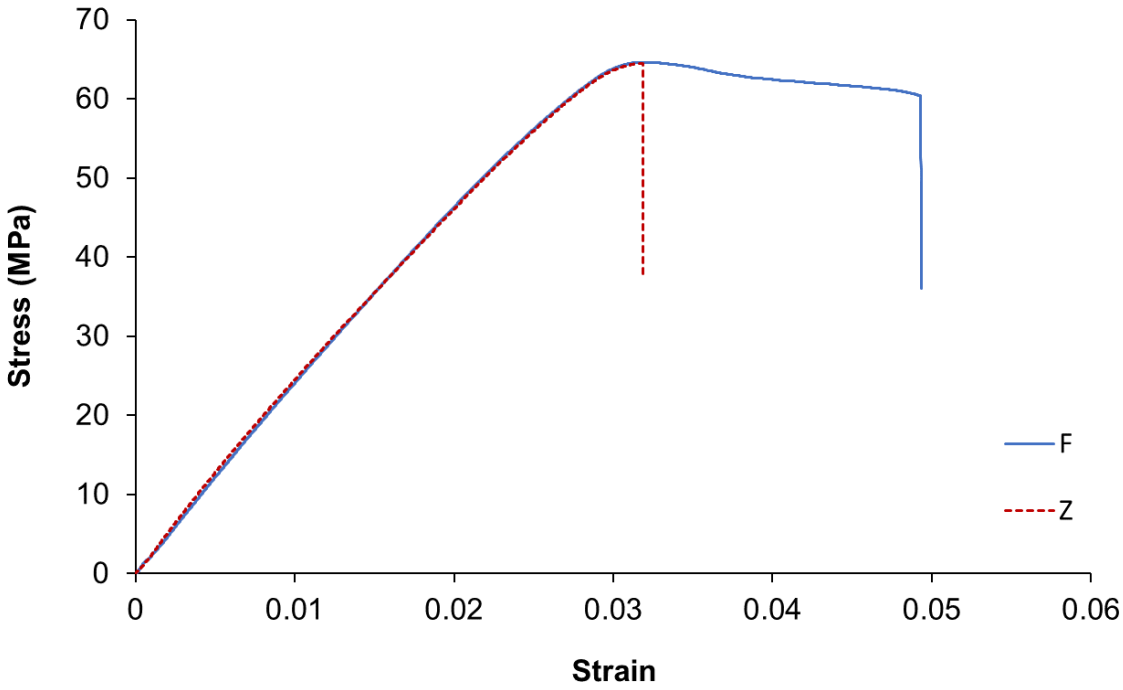


**Fig. 8** *Stress-strain curves for one representative specimen in each orientation (F and Z) for specimens with the reference geometry (0.2 - 0.5).*

*Summary*

Analysis of strength in F and Z specimens of PLA indicate that both orientations achieved bulk-material strength. The strength of the interface was equivalent to that of the filament, indicating that the bonding between layers was sufficient to give bulk-material performance.

Additionally, this finding translated across a wide range of filament geometries (variable LH, EFW and aspect ratio), which would have significantly affected the flow and thermal history of the polymer. For instance, the volumetric extrusion rate and cross-sectional area of extruded filaments varied by up to two times, affecting shear stress during extrusion, cooling rates and many other factors. This demonstrates the robustness of the findings and supports the theory [25] that a bulk-strength interface is feasible. Irrespective of extruded filament geometry, the time above the glass

transition temperature during the deposition process was sufficient to enable adequate reptation to provide the bulk-material performance in all specimen types.

The study of the effect of the cross-sectional surface area on maximum tensile load demonstrated that the load-bearing capacity of specimens correlated directly with the area of the material. These results indicate that it is reasonable to consider the specimen as a single bulk material – without weak interfaces between its layers- and the major factor contributing to anisotropy in MEAM-generated parts is filament-scale geometry, which should be more closely examined as a contributor to mechanical-performance limitations.

### 3.2 Strain-at-fracture and toughness

This section considers the effect of filament-scale geometry on strain-at-fracture and toughness of 3D-printed PLA, using FEA simulations to support analysis of experimental results.

*Strain-at-fracture*

In contrast to strength, which was found to be similar for all extruded filament geometries, a significant difference was observed for strain-at-fracture between F-direction and Z-direction specimens (Fig. 9 (a) and (b), respectively). One F-0.15-0.5 specimen did not fail during testing up to a strain of 0.2. Apparently, all Z specimens fractured at significantly lower strains compared to F specimens. Z specimens across both groups were in a strain-at-fracture range from 0.017 to 0.033, while F specimens demonstrated a greater range - 0.038 to 0.2. This can be explained by strain localisation in the interface regions of Z specimens, which resulted in rapid and sudden fracture at lower overall strain values (discussed in the FEA section below). In F specimens, strain-at-fracture was more representative of bulk properties of PLA, which was demonstrated to range between 0.02 and 0.16 in [13,29–35].

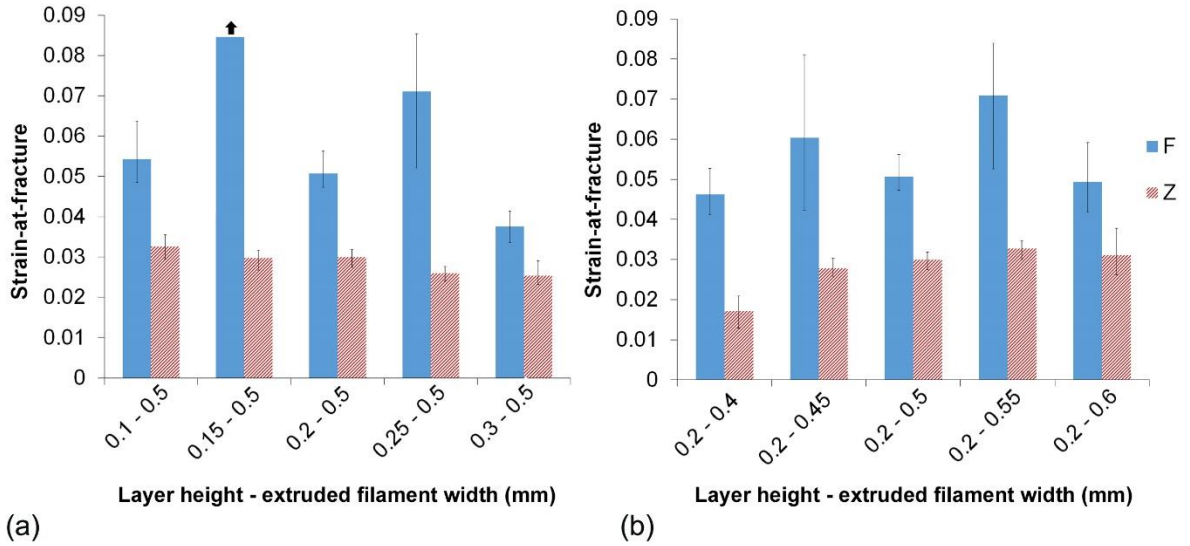


**Fig. 9** *Strain-at-fracture of F and Z specimens, with varying LH (a), and with varying EFWs (b). Two F-0.15-0.5 specimens failed to fracture as indicated by the arrow in (a). Error bars indicate the range of values for six specimens.*

In Z specimens, it was observed that mean strain-at-fracture values decreased continuously from 0.033 to 0.025 as LH increased (Fig. 9 (a)). This parameter diminished from 0.031 to 0.017 as EFW decreased (Fig. 9 (b)), indicating a dependence of strain-at-fracture on filament geometry.

To investigate the effect of filament geometry on stress concentration, the bond angle was measured for all specimens. As demonstrated in Fig. 10 (a) and (b), the bond angle between layers in Z specimens varied depending on extruded filament geometry. As the LH increased, the mean bond angle decreased from 87.6 to 64.4° (Fig. 10 (a)). As the EFW decreased, the bond angle decreased from 80.1 to 66.2° (Fig. 10 (b)). The values of strain-at-fracture are plotted against the respective bond angles in Fig. 10 (c), demonstrating a relationship between the geometry of the interface (bond angle) and mechanical performance (strain-at-fracture). Inset micrographs in Fig. 10 (c) show examples of bond-angle measurements for two extruded filament geometries. These results indicate that the extruded filament geometry contributes towards an increased stress/strain concentration, analysed in the next Section.

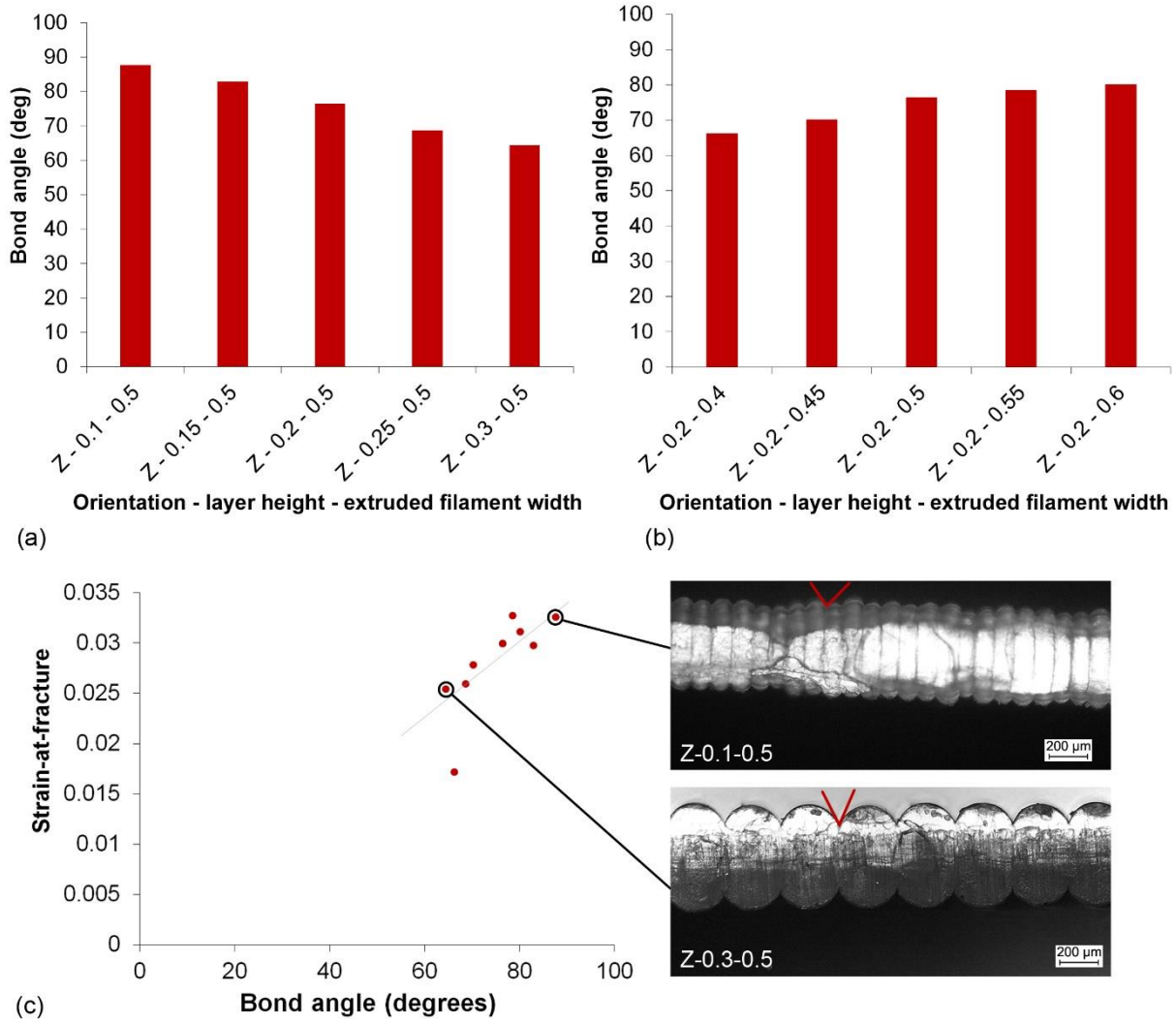


**Fig. 10** *Effects of LH (a) and EFW (b) on bond angle. (c) Relationship between bond angles and strain-at-fracture. Inset microscopy demonstrates the variation in bond angles of Z specimens with different filament geometries.*

*FEA of strain concentration*

The previous sections showed strain-at-fracture - but not strength - to be dependent on extruded filament geometry. It may be expected that stress concertation (due to grooves between extruded filaments that are subject to tensile separation) affect both strength and strain-at-fracture in similar ways. Therefore, FEA simulations were conducted to understand this. An elastic/perfectly-plastic material model was used for PLA, based on geometry of the reference F specimen (F-0.2-0.5). It was found that during the elastic loading phase, concentrations of stress and strain were identical, as

would be expected. However, after the material yielded, the maximum value of stress no longer increased (stress concentration decreased since mean stress continued to increase after local yielding), whereas strain increased more easily, and, therefore, strain concentration began to increase rapidly. This can be seen from the FEA results in Fig. 11 (a), where strain concentration increased by approximately 50% as applied strain increased from 0% to 2%, but increased by over 400% as applied strain increased from 2% to 4%. The images of FEA results (i) and (ii) in Fig. 11 (b) show strain concentration plots in the elastic and elastic-plastic regimes, respectively.

Since experimental bond strength was similar to that of the bulk material, the material in this study (PLA) was apparently ductile enough to achieve the strain necessary for UTS in Z specimens, even with the presence of strain/stress concentrations. To investigate this, the experimental results for bulk-material strain-at-fracture (6% to 25%; from F specimens) were used to determine the blue region in Fig. 11 (a), which indicates the strain concentration at which material failure may be expected. The normalisation of FEA and experimental data were carried out by dividing the values by the applied strain (e.g. 0.005, 0.01, 0.015 etc). Intersections of the red (FEA) line with the blue region correspond to the levels of localised strain sufficient for failure. The values of applied strain at which failure were predicted with FEA - 0.015 to 0.025 (vertical dashed lines in the figure) - are similar to those observed in experimental Z specimens - 0.017 to 0.033. This indicates that the local levels of strain-at-fracture (due to strain concentration) may be similar to strain-at-fracture for the bulk material. This, once more, supports the hypothesis that the bonds have bulk-material properties and the observed anisotropy of 3D-printed MEAM specimens is caused by filament-scale geometry.

A robust finding of this FEA analysis is that strain concentration increases exponentially as applied strain increases (in contrast to decreasing stress concentration). This explains the difference in trends between strength and strain-at-fracture in the previous sections. It can also explain narrower errors bars of Z specimens compared to F specimens for strain-at-fracture in Fig. 9; acceleration of strain concentration meant that small increases in applied strain achieved large increases in local strain.

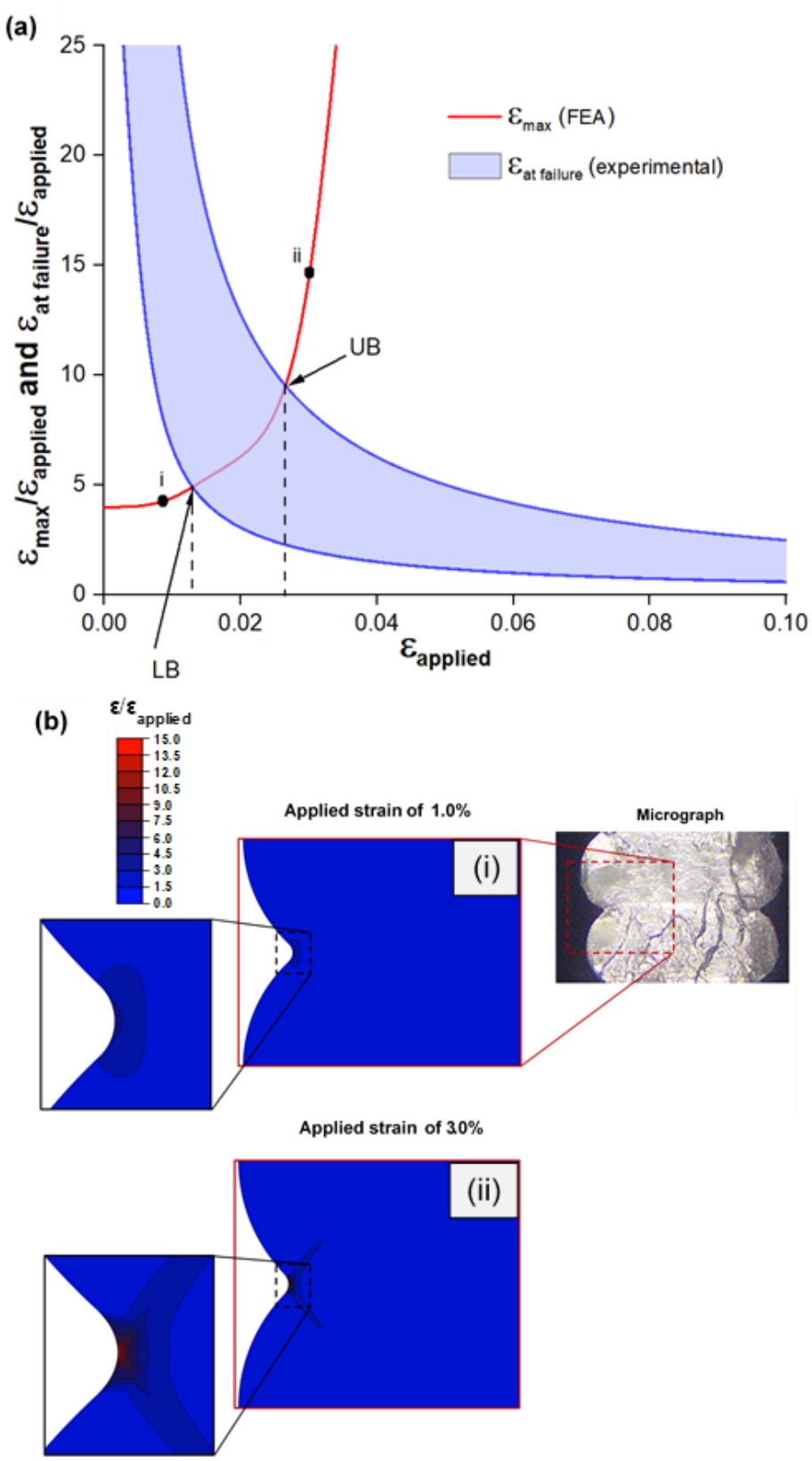


**Fig. 11** *(a) Effect of applied strain on calculated (with FEA simulations – red line) and estimated strain concentration required for material failure (based on experimental results – blue shaded region). The lower (LB) and upper (UB) boundaries are based*

*on the experimental range of strain-at-fracture and indicate the potential onset of strain localisation and failure. (b) Evolution of strain concentration with increase of applied strain from 1.0% (i) to 3.0% (ii) strain for Z-0.2-0.5 specimen.*

*Toughness*

Assessment of toughness of all specimens (Fig. 12) indicated that F direction have a significantly greater toughness than Z specimens. The mean toughness of F specimens was 2.74 J $mm^{-3}$, while that of Z specimens achieved only 35.6% of this level (mean value of 0.98 J $mm^{-3}$). As with strain-at-fracture, F-0.15-0.5 was not considered as two of specimens failed to fracture during testing. Generally, F specimens outperformed Z ones. This supports the findings for strain-at-fracture, indicating that the filament-scale geometry reduces the mechanical performance significantly.

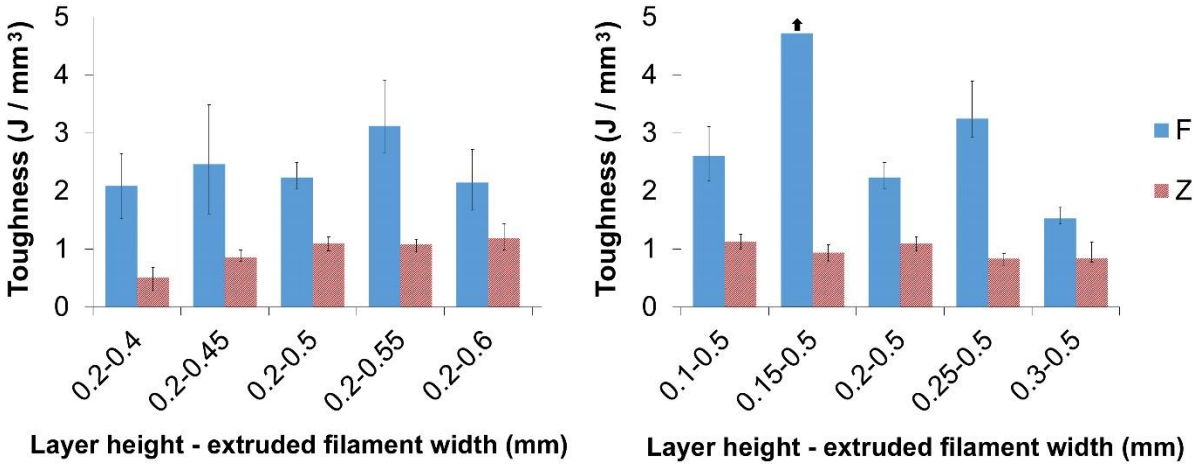


**Fig. 12** T*oughness of F and Z specimens with various LH (a) and EFWs (b). Two F-0.15-0.5 specimens failed to fail (indicated by the arrow in (a)). Error bars indicate the range of values for six specimens.*

### 3.3 Specific load-bearing capacity

Strength of the bond between layers was shown above to be similar to that of the bulk material. However, even if the whole structure is considered as bulk material without weak interfaces, its geometry obviously impacts the load that can be sustained. Hence, the F specimens typically sustained more load that the Z specimens, as was discussed in relation to Fig. 7. To understand the effect of structural integrity related to geometries and orientations of extruded filaments, specific load-bearing capacity (the maximum load of specimen normalised by the weight of the unit length of the specimen gauge) is investigated in this section. This section analyses the effects of LH, EFW and aspect ratio on specific load-bearing capacity and then characterises the cross-sectional area that is effectively available for sustaining applied loads.

*LH*

The F-direction specimens demonstrated very similar mean specific load-bearing capacity at all LHs (Fig. 13 (a)) within a narrow range of ±3.4%. In contrast, the Z specimens exhibited a significantly reduced specific load-bearing capacity as compared to their F counterparts and its significantly broader range - ±14.9%. A trend was observed in Z specimens with regards to the effect of layer-height variation: the three specimens with a LH of 0.2 mm or less attained similar specific load-bearing capacities, but a decline of this parameter was seen for specimens with LH above 0.2 mm. The plateau in performance indicates that there may be a threshold (0.2 mm) for the chosen printing parameter, below which the specimen LH performs optimally (see also discussion in relation to aspect ratio below).

*EFW*

The F specimens with different EFW demonstrated consistent specific load-bearing capacity, with a relatively narrow range of ±6.9% for the mean values of the five specimen types (Fig. 13 (b)). As with the LH, Z specimens again showed a reduced specific load-bearing capacity and significantly more variability, with range of ±23.5%. Here, above an EFW of 0.4 mm, specific load-bearing capacity of Z specimens

plateaued. A 37% decline in performance was found as the EFW reduced from 0.45 mm to 0.4 mm (Fig. 13 (b)).

*Aspect ratio*

Trends in the previous two sections suggest that the aspect ratio may have an important effect on specific load-bearing capacity, since both the increase in the EFW and the reduction of the LH caused its increase. By combining all results together, it can be seen (Fig. 13 (c)) that Z specimens with an aspect ratio below 2.5 demonstrated a rapid and significant decline in specific load-bearing capacity as the aspect ratio decreases. For aspect ratios in excess of 2.25 the specific load-bearing capacity performance in Z direction plateaued and remained relatively constant (a range of ±5.8% for the aspect ratios between 2.25 and 5), indicating optimal performance. This finding demonstrates that the LH and the EFW have a combined effect on mechanical performance. Sub-optimal aspect ratios resulted in reduced mechanical performance of the Z specimens. As previously discussed, the F specimens displayed very similar performance across the range of aspect ratios considered, with a narrow range of ±3.4%; demonstrating that the printing process did not affect the material properties. These results are examined in more detail in the next section, dealing with the effect of extruded filament geometry and orientation on the relative load-bearing area and its influence on mechanical performance.

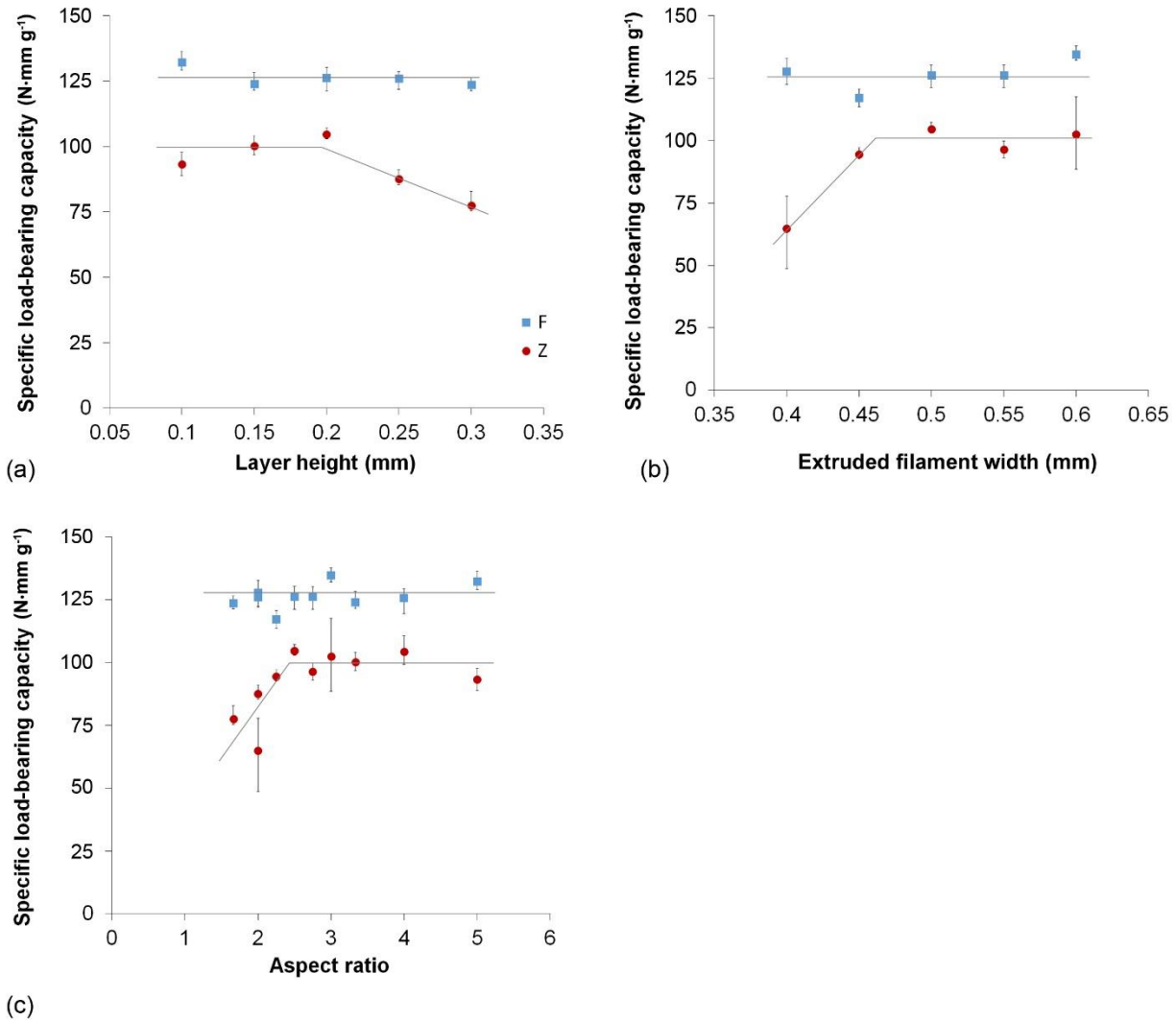


**Fig. 13** *(a) Effect of LH on specific load-bearing capacity of F and Z specimens (EFW 0.5 mm). (b) Effect of EFW on specific load bearing capacity of F and Z specimens (LH 0.2 mm). (c) Effect of aspect ratio on specific load bearing capacity of all F and Z specimens. Error bars indicate the range of values for six specimens.*

*Relative load-bearing area*

As presented in the previous sections and illustrated in Fig. 13 (a) - (c), there is a significant difference between the specific load-bearing capacity of F and Z specimens, even though bonds with bulk-material strength were shown in Section 3.1. In the case of the F specimens, the combined load-bearing capacity of all extruded filaments (loaded in the direction of filaments) contribute to the load-bearing capacity of the part. So, minor variations in extruded filament geometry have a low impact on

the cross-sectional area and specific load-bearing capacity remains very similar for all specimen geometries. However, specific load-bearing capacity of the Z specimens is defined by the narrowed interfacial regions between extruded filaments, resulting in a reduced specific load-bearing capacity. The combined mean value for all Z specimens was 28.7% lower than F specimens (94.5 versus 126.5 $N \cdot mm\ g^{-1}$).

To investigate the causes of this difference, a relative load-bearing area (%) is considered here, defined as the fraction of the cross-sectional surface area that sustains load in the narrowest region (where fracture occurs) (related to the average cross-sectional area). The mean relative load-bearing area of all Z direction specimens was 26.0% lower than that of all F specimens (Fig. 14 (a)) due to the presence of narrower interface bonds (shown schematically in Fig. 14 (f) and (g)). In the F specimens, interfaces did not reduce the load-bearing area (Fig. 14 (c) and (d)), and therefore, the relative load-bearing area is close to 100% (potentially slightly lower due to minor geometrical fluctuations). The two examples circled in Fig. 14 (a) and shown in Fig. 14 (e) and (h) demonstrate the difference in relative load-bearing areas for specimens with equivalent geometries (F-0.3-0.5 and Z-0.3-0.5) but tested in different - F and Z - orientations. F-0.3-0.5 specimens had a mean relative load-bearing area of 94.5%, whereas the Z specimens had 64.8%.

The FEA results in Fig. 15 present the distribution of von Mises stress in the Z specimens, demonstrating realisation of the concept shown schematically in Fig. 14 (g) in tested specimens. The three models in Fig. 15 reproduced the geometries obtained with microscopy for three Z specimens with the same EFW (0.5 mm) but different LHs; 0.1 mm, 0.2 mm and 0.3 mm. As the LH increased, the width of the region predominantly sustaining the applied load (higher von Mises stress) reduced, as indicated by narrower “region B” in Fig. 15 (a) and wider one in Fig. 15 (c). Apparently, regions of the extruded filament that protrude beyond the interfacial bonded regions are subject to low stresses. This highlights the fact that non-load-bearing areas in the Z specimens (Fig. 14 (d)) are effectively a wasted material (in terms of sustaining loads), but still contribute to the weight of the specimen. This is further evidenced in the microscopy of fracture surfaces of F and Z specimens (Fig. 14 (e) and (h), respectively), which show the relative load-bearing areas of a small section in each case.

Fig. 14 (b) indicates that, as expected, specific load-bearing capacity did not depend on the cross-sectional area for the F specimens as schematically shown in Fig. 14 (e). For Z specimens, however, the specific load-bearing capacity increased as fracture surface area increased (measured with microscopy), indicating that wider extruded filaments have more effective structural geometry for sustaining loads, and demonstrating that it may be advantageous to design the toolpath strategy to achieve wide extrusions. A threshold surface area may exist for Z specimens, above which specific load-bearing capacity no longer improves; this is logical since, at large EFWs (or low LH), the load-bearing area would approach 100%.

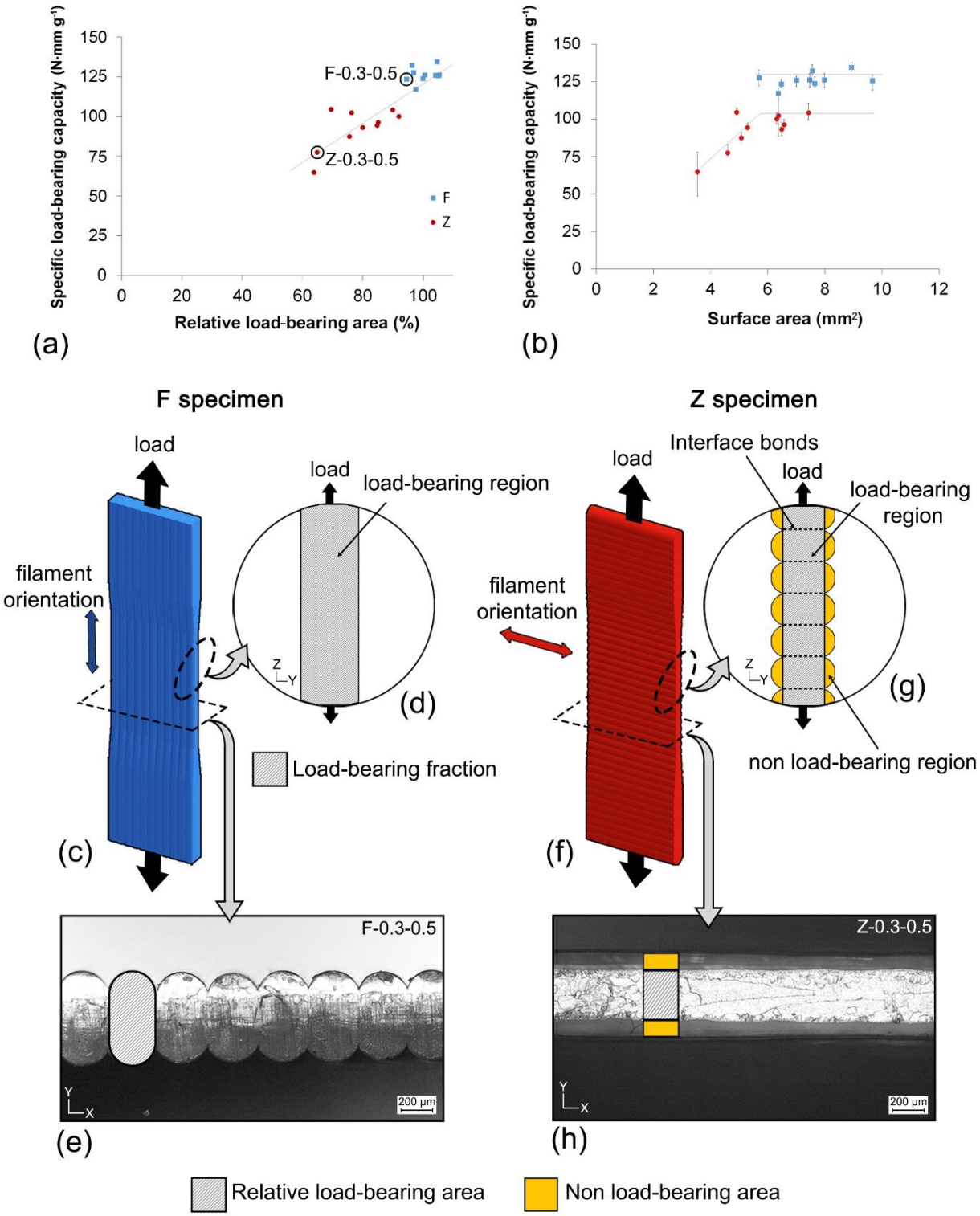


**Fig. 14** *(a) Relationship between specific load-bearing capacity and mean relative load-bearing area (fraction of cross-sectional surface area that sustains the applied load). Error bars indicate the range of values achieved by six specimens. (b) Relationship between specific load-bearing capacity and surface area. (c) Schematic of F specimen with longitudinal cross-sectional inset (d) showing load-bearing region*

*and microscopy of transversal cross-section (e) demonstrating relative load-bearing area. (f) Schematic of Z specimen type with longitudinal cross sectional inset (g) showing load-bearing region and microscopy of transversal cross-section (h) demonstrating relative load-bearing area.*

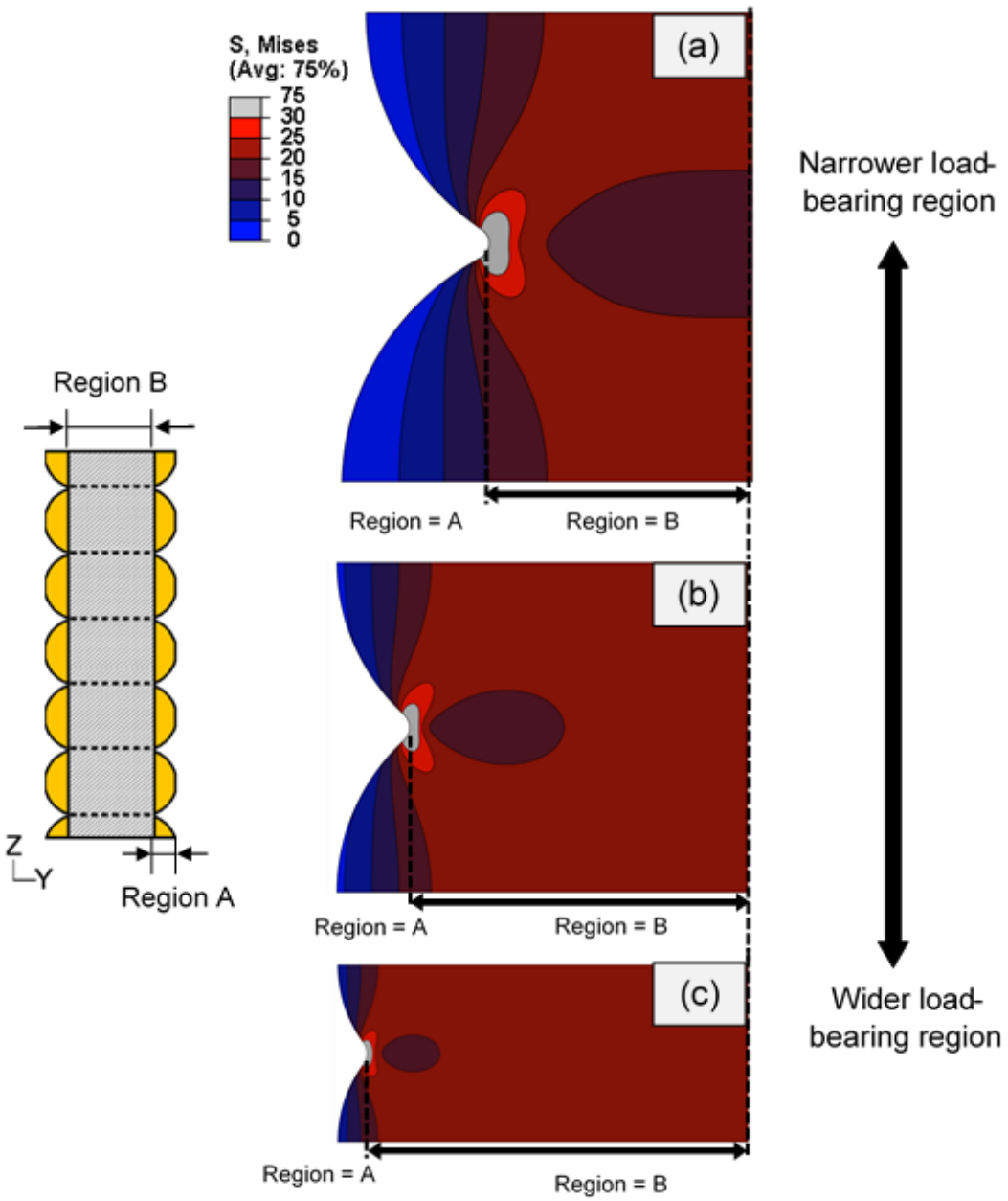


**Fig. 15** *Distribution of von Mises stress for Z specimens with the same EFW (0.5 mm) and different LH: 0.3 mm (a), 0.2 mm (b) and 0.1 mm (c). As the interface gets wider,*

*the load-bearing region increases as opposed to region of reduced loading (region A), indicated by the lower von Mises stress.*

*Summary*

The mechanical performance of the Z specimens was reduced compared to that of the F due to the presence of geometric features (grooves naturally occurring in 3D printing) at the filament scale, not due to poor interfacial bonding as is commonly attributed in the literature. In these specimens, the geometric features occur in the region of interface, causing reduced levels of relative load-bearing area and load-bearing capacity. In the F specimens, filament-scale geometry does not affect the mechanical performance because their grooves are oriented parallel to the loading direction.

### 3.4 Applicability of results

This section utilises the results from Section 3.1 - 3.3 and suggests a way of their utilisation for parameter selection for MEAM. They are also applied to previous studies to enable new understanding of anisotropy of MEAM-manufactured parts.

*Ashby plots*

Ashby plots [36] were utilised to combine the results for all specimens into performance maps. The first (Fig. 16 (a)) demonstrates the link between strength and strain-at-fracture for varying the extruded filament geometry in both F and Z specimens. The second (Fig. 16 (b)) relates the specific load-bearing capacity and strain-at-fracture. In addition to providing valuable data about the effects of LH, EFW and orientation, these plots are useful for assessing the performance of all specimens manufactured to select the filament orientation in order to attain a desired strength, specific load-bearing capacity or strain-at-fracture to meet demands of specific mechanical applications.

Apparently, the F specimens all share similar strength (Fig. 16 (a)) irrespective of EFW or LH, with a relatively narrow range (57.67 to 71.58 MPa). However, there is a broader range of strain-at-fracture values (0.036 to 0.085); more than twofold increase

between the smallest and largest values, not uncommon in polymers. The Z specimens, on the other hand, demonstrate a narrower range of strain-at-fracture values (0.013 to 0.038) but a greater variation in strength (38.58 to 69.88 MPa). Numerous Z specimens achieved maximum strength values that were comparable to F direction, but only a very limited number demonstrate similar capabilities in strain-at-fracture, when compared with the F specimens, due to increased localised strain in the former caused by the interface bond geometry. The map (Fig. 16 (a)) also establishes that both F and Z specimens share similarities with bulk PLA according to numerous studies [13,29–35], in terms of material strength, but with the reduced strain-at-fracture capabilities of the Z specimens.

In terms of specific load-bearing capacity (Fig. 16 (b)), unlike the first map (Fig. 16 (a)), the Z specimens showed a significantly reduced mechanical performance as compared to the F ones, with no overlap between domains for the two orientations. This highlights the major difference between the mechanical performance of specimens oriented in F and Z direction: while they share rather similar characteristics of strength, resulting from the material in the region of interface performing similarly to that of the extruded filament in the F direction, the significant difference in strain-at-fracture and specific load-bearing relates to the reduced geometrical effectiveness of extruded filaments in the Z direction specimens. This emphasises the importance of extruded filament orientation when considering mechanical applications of MEAM-generated parts. Bulk-material properties are not shown in Fig. 16 (b) since the load-bearing capacity directly depends on overall specimen geometry.

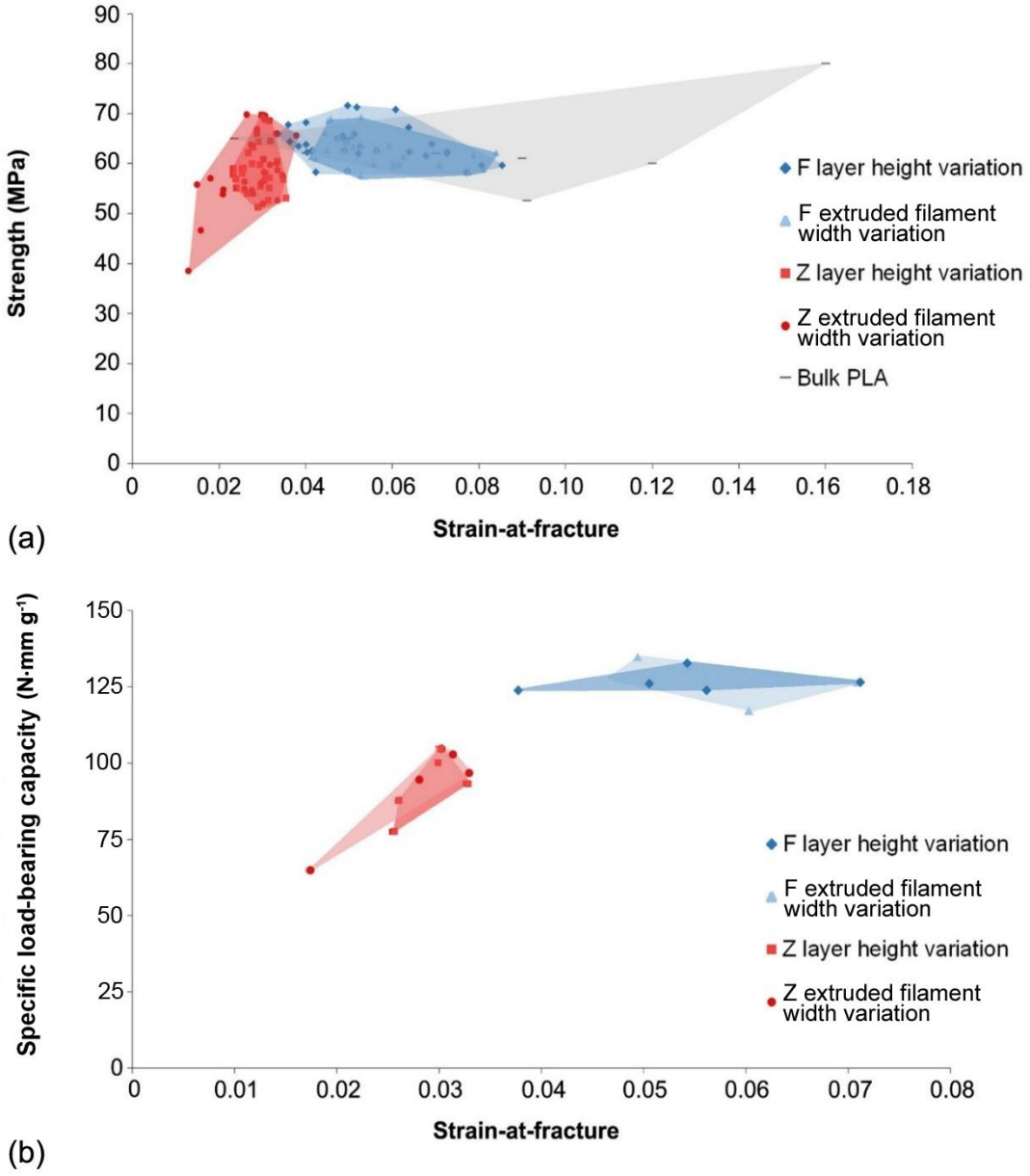


**Fig. 16** *(a) Strength - strain-at-fracture maps of tested specimens. In addition, bulk PLA properties from previous studies are plotted. (b) Maps of specific load bearing capacity versus strain-at-fracture of tested specimens.*

*Application of relative load-bearing area to previous studies*

Z-direction strength of MEAM specimens is consistently reported as being lower than F-direction strength, which is often attributed to interfacial bond weakness. This study has demonstrated the strength of the interface to be equivalent to both filament-direction and bulk-material strengths. So, it was hypothesised that the new

understanding of bond geometry developed in this study could be used to predict the bond strength in other studies that did not consider the area of the bond. In this way it is possible to determine whether interfaces in previous studies also had bulk strength. The method developed for this assessment was as follows:

(1) Cross-sectional areas of the test specimens were calculated from the dimensions reported in the reviewed study.

(2) The applied load was calculated by multiplying the reported strength by cross-sectional area.

(3) The filament geometry (in terms of LH and EFW) was cross-referenced with the present study to find the equivalent extruded filament geometry, from which the relative load-bearing area (Fig. 14 (a)) was defined.

(5) The reported cross-sectional area was multiplied by the relative load-bearing area to give a revised cross-sectional area, i.e. the area of the interface between extruded filaments.

(6) The calculated load was divided by the revised cross-sectional area to give the bond strength.

To apply this method, a review of the literature was undertaken. Studies providing details of specimen's dimensions and extruded filament geometry (LH and EFW), or for which the data could be derived (microscopy, volumetric flow rates, etc.) were considered. Any studies, which did not use extruded filament geometries similar to those of the present study, were excluded. Four studies were identified that complied with the criteria: two studies of PLA [13,24] and two of ABS [19,37]. Utilising the recalculation method detailed above, the revised strength increased in all studies and fell within the range for bulk materials indicated in the literature [11,12,38–41,13,29–35] (Fig. 17 (a) - (d)).

To further validate this method, the strength of the reference Z specimen from this study (Z-0.2-0.5) was recalculated using a digital caliper to measure the specimen width (instead of determining the bonded area between extruded filaments from micrographs) as done in most studies. The strength was found to be 40.6 MPa, a 38.15% decrease of the level of 65.6 MPa calculated using the bonded area between

extruded filaments, indicating the same (but opposite trend) to the two studies of PLA utilised for the recalculation (41.1 MPa and 48 MPa).

The results of this section demonstrate that the Z-direction weakness found in many studies may be solely due to geometric factors as opposed to sub-optimal healing of the bond between layers, as often reported. Apparently, the findings of the present study can be used to develop a new understanding of the previous studies.

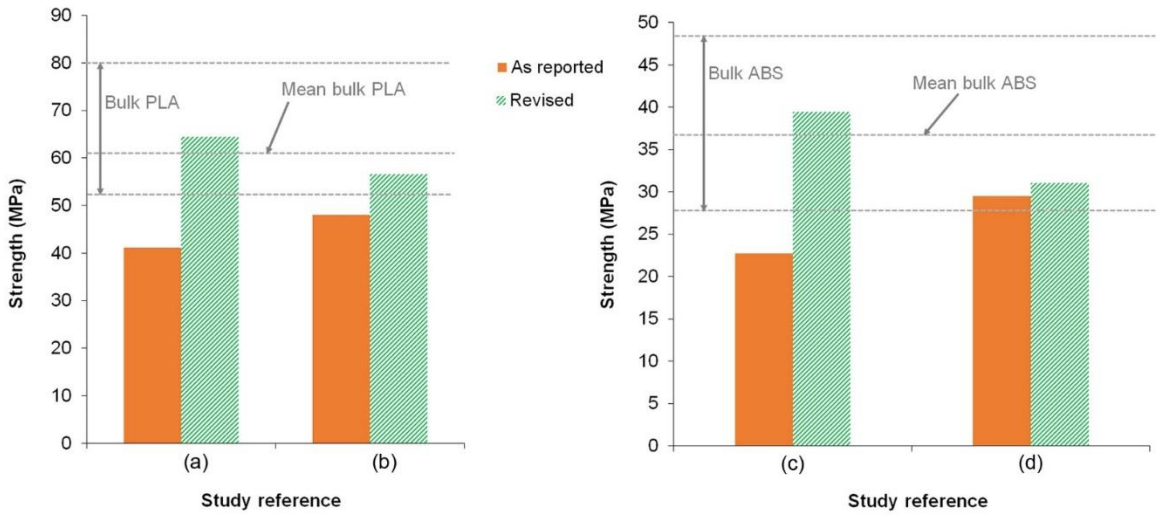


**Fig. 17** *As-reported and revised strength values for previous studies of MEAM-generated PLA (a) [24] and (b) [13], and ABS (c) [19] and (d) [35] specimens.*

*Applicability to different layer times and printing speeds*

To demonstrate the robustness of this study's findings, data from an ongoing investigation into the effects of printing speed and layer times on interlayer bond strength are shown in Fig. 18. The data were obtained for the same extruded-filament geometry as that of the reference specimen Z-0.2-0.5, but the printing speed (speed at which the nozzle moved in X-Y plane) and the layer time (time taken to print each layer) were changed independently. The level of speed was changed from the reference speed of 1000 mm $min^{-1}$ to higher (1200 mm $min^{-1}$) or lower (800 mm $min^{-1}$) ones. The layer time was changed to be 50% longer or 50% shorter by varying the length of the box walls. All other elements of the used methodology were kept the same as outlined in Section 2. No significant changes in strength associated with either print speed or layer time were found. This indicates that the main findings of this

study are not sensitive to deposition-related thermal factors, given that there was up to a threefold increase in cooling time between printing at the same position on consecutive layers. The range of mean strengths for all specimens in this study (in both F and Z directions) is shown in Fig. 18, emphasising that bulk-strength interlayer bonding was achieved for different speeds/layer times, and that the findings of this study are robust with regard to these factors.

In relation to other studies, the cross-sectional area of the box specimens in this study (72 - 108 $mm^2$) was larger than that of ASTM D638 Type I, II, IV and V specimens (at least 4x larger than Type IV and at least 7x larger than Type V). Therefore, the time between the layers in this study (approximately 10 - 11 seconds) may be lower than that in many studies with ASTM D638 tensile testing specimens printed in the upright (Z) orientation. For larger industrial parts, layer times may be much longer, and this could affect interlayer adhesion, although the findings in this study for microscale geometric effects will still apply. It should also be noted that excessively high print speeds may lead to issues related to fidelity or a range of other defect types, which were deliberately excluded here thanks to the simple continuous toolpath design used to develop fundamental understanding of the process. It is also important to highlight that the cross-sectional areas of different extruded-filament geometries in this study differed by more than twofold, and, therefore, the thermal conditions of conduction/cooling would have been considerably different. Still, this did not affect the bond strength.

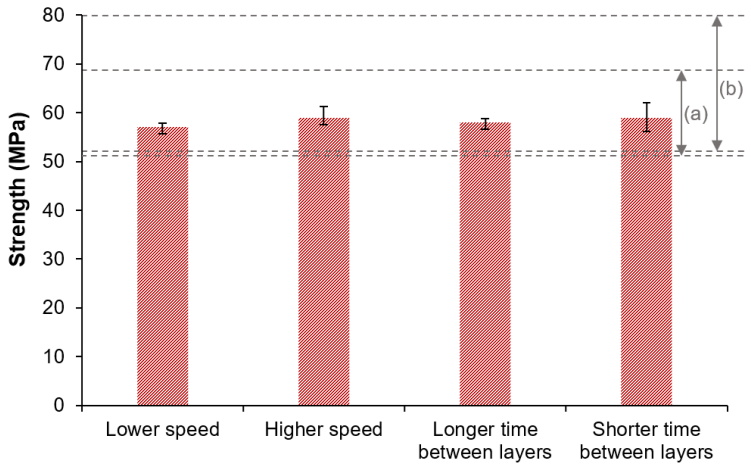


**Fig. 18** *Strength of specimens manufactured at lower/higher speeds and with longer/shorter times between layers (6 replicates). The dashed lines indicate the range (a) of mean strengths of all other specimen types (F or Z) in this study and (b) bulk strength PLA as reported in existing studies.*

*Application to other materials, industrial applications and future research*

This study considered PLA, but the results of the previous section show that the findings may translate to ABS. Preliminary investigations (unpublished data) suggest that the results for a bulk-strength interface are also applicable for polyamide, and further research is ongoing.

This research indicates that to enhance mechanical performance, future research efforts should be focussed on improving geometrical strategies to overcome constraints of anisotropic behaviour resulting from filament-scale geometries (as opposed to poor interface bonding). In addition, MEAM-produced specimens should be analysed geometrically at the scale of individual extruded filaments. The new specimen design highlights the benefit of simplifying the toolpath design to develop fundamental understanding. It allows fundamental research into a wide range of factors that are likely to affect mechanical or thermal behaviours such as nozzle temperature, polymer molecular weight, environment temperature and active cooling (nozzle-mounted-fan speed).

In the longer term, the results may help to improve the design of industrial parts by understanding the cause of anisotropic properties and either addressing the limitations or optimising designs to minimise their impact. Parts oriented in the direction of extruded filaments significantly outperform those along the Z-direction in specific load-bearing capacity, strain-at-fracture and toughness. This indicates that parts generated with MEAM for the purpose of mechanical loading should be manufactured with the extruded filaments oriented predominantly in the direction of loading in order to achieve the bulk-material performance. Ongoing research by the authors focuses on the applicability of findings to larger structures with more complex toolpaths (as opposed to single-filament-wide specimens) and established that unconventional toolpath strategies might result in the improved Z-direction performance by modifying the filament-scale structural geometry.

## 4 Conclusions

This study identified that the strength of the filament (F direction) and the strength of the interface bond (Z direction) of PLA specimens produced with MEAM were both

similar to that of the bulk material. Extruded-filament-geometry modifications (LH, EFW and aspect ratio) had a very limited effect on the strength. In contrast, the strain-at-fracture, specific load-bearing capacity and toughness were greater in F direction than in Z direction due to the presence of filament-scale geometric features (narrowing) in the region of the interface bond and a reduction in a relative load-bearing area in the Z specimens. FEA simulations supported and confirmed the experimental findings. A method to apply the results of this study to further analyse existing literature data was developed and showed that bulk-material performance might occur in previous studies, and, therefore, their anisotropy resulted solely from geometric factors. Additionally, this study demonstrated that modifications to print speed and layer times had no effect on the strength of the interlayer bond. The results in this study were obtained by studying mechanical properties with a specially designed specimen (comprising individually bonded extruded filaments with variable widths achieving a dogbone shape) and allowed new fundamental understanding of mechanical anisotropy reported for MEAM to be developed, which has not been published previously, to the knowledge of the authors.

## 5 Acknowledgements

This research did not receive any specific grant from funding agencies in the public, commercial, or not-for-profit sectors.

## References

[1] P. Honigmann, N. Sharma, B. Okolo, U. Popp, B. Msallem, F.M. Thieringer, Patient-specific surgical implants made of 3D printed PEEK: Material, technology, and scope of surgical application, Biomed Res. Int. 2018 (2018). https://doi.org/10.1155/2018/4520636.

[2] K.C. Wong, 3D-printed patient-specific applications in orthopedics, Orthop. Res. Rev. Volume 8 (2016) 57–66. https://doi.org/10.2147/ORR.S99614.

[3] S. Ahn, M. Montero, D. Odell, S. Roundy, P.K. Wright, Anisotropic material properties of fused deposition modeling ABS, Rapid Prototyp. J. 8 (2002) 248–257. https://doi.org/10.1108/13552540210441166.

[4] O.S. Es-Said, J. Foyos, R. Noorani, M. Mendelson, R. Marloth, B.A. Pregger,

Effect of layer orientation on mechanical properties of rapid prototyped samples, Mater. Manuf. Process. 15 (2000) 107–122. https://doi.org/10.1080/10426910008912976.

[5] A.K. Sood, R.K. Ohdar, S.S. Mahapatra, Improving dimensional accuracy of Fused Deposition Modelling processed part using grey Taguchi method, Mater. Des. (2009) 4243-4352. https://doi.org/10.1016/j.matdes.2009.04.030.

[6] I. Durgun, R. Ertan, Experimental investigation of FDM process for improvement of mechanical properties and production cost, Rapid Prototyp. J. 20 (2014) 228–235. https://doi.org/10.1108/RPJ-10-2012-0091.

[7] J.P. Thomas, J.F. Rodríguez, J.E. Renaud, Mechanical behavior of acrylonitrile butadiene styrene (ABS) fused deposition materials. Experimental investigation, Rapid Prototyp. J. 7 (2001) 148–158. https://doi.org/10.1108/13552540110395547.

[8] J.C. Riddick, M.A. Haile, R. Von Wahlde, D.P. Cole, O. Bamiduro, T.E. Johnson, Fractographic analysis of tensile failure of acrylonitrile-butadiene-styrene fabricated by fused deposition modeling, Addit. Manuf. 11 (2016) 49–59. https://doi.org/10.1016/j.addma.2016.03.007.

[9] V.E. Kuznetsov, A.N. Solonin, O.D. Urzhumtsev, R. Schilling, A.G. Tavitov, Strength of PLA components fabricated with fused deposition technology using a desktop 3D printer as a function of geometrical parameters of the process, Polymers (Basel). 10 (2018). https://doi.org/10.3390/polym10030313.

[10] C. Koch, L. Van Hulle, N. Rudolph, Investigation of mechanical anisotropy of the fused filament fabrication process via customized tool path generation, Addit. Manuf. 16 (2017) 138–145. https://doi.org/10.1016/j.addma.2017.06.003.

[11] S. Ziemian, M. Okwara, C.W. Ziemian, Tensile and fatigue behavior of layered acrylonitrile butadiene styrene, Rapid Prototyp. J. 21 (2015) 270–278. https://doi.org/10.1108/RPJ-09-2013-0086.

[12] T.J. Coogan, D.O. Kazmer, Bond and part strength in fused deposition modeling, Rapid Prototyp. J. 23 (2017) 414–422. https://doi.org/10.1108/RPJ-03-2016-0050.

[13] M. Spoerk, F. Arbeiter, H. Cajner, J. Sapkota, C. Holzer, Parametric optimization of intra- and inter-layer strengths in parts produced by extrusion-based additive manufacturing of poly(lactic acid), J. Appl. Polym. Sci. 134 (2017). https://doi.org/10.1002/app.45401.

[14] B. V. Reddy, N. V. Reddy, A. Ghosh, Fused deposition modelling using direct extrusion, Virtual Phys. Prototyp. 2 (2007) 51–60. https://doi.org/10.1080/17452750701336486.

[15] N. Aliheidari, J. Christ, R. Tripuraneni, S. Nadimpalli, A. Ameli, Interlayer adhesion and fracture resistance of polymers printed through melt extrusion additive manufacturing process, Mater. Des. 156 (2018) 351–361. https://doi.org/10.1016/j.matdes.2018.07.001.

[16] C. Bellehumeur, L. Li, Modeling of bond formation between polymer filaments in the fused deposition modeling process, J. Manuf. Process. 6 (2004) 170–178. https://doi.org/10.1016/S1526-6125(04)70071-7.

[17] F. Ning, W. Cong, Y. Hu, H. Wang, Additive manufacturing of carbon fiber-reinforced plastic composites using fused deposition modeling: Effects of process parameters on tensile properties, J. Compos. Mater. 51 (2016) 451–462. https://doi.org/10.1177/0021998316646169.

[18] K.G.J. Christiyan, U. Chandrasekhar, K. Venkateswarlu, A study on the influence of process parameters on the mechanical properties of 3D printed ABS composite, IOP Conf. Ser. Mater. Sci. Eng. 114 (2016). https://doi.org/10.1088/1757-899X/114/1/012109.

[19] A.C. Abbott, G.P. Tandon, R.L. Bradford, H. Koerner, J.W. Baur, Process-structure-property effects on ABS bond strength in fused filament fabrication, Addit. Manuf. 19 (2018) 29–38. https://doi.org/10.1016/j.addma.2017.11.002.

[20] A.Q. Pan, Z.F. Huang, R.J. Guo, J. Liu, Effect of FDM process on adhesive strength of polylactic acid (PLA) Filament, Key Eng. Mater. 667 (2015) 181–186. https://doi.org/10.4028/www.scientific.net/KEM.667.181.

[21] T.J. Coogan, D.O. Kazmer, Healing simulation for bond strength prediction of FDM, Rapid Prototyp. J. 23 (2017) 551–561. https://doi.org/10.1108/RPJ-03-

2016-0051.

[22] G. Onwubolu, F. Rayegani, Characterization and optimization of mechanical properties of ABS parts manufactured by the fused deposition modelling process, 2014 (2014) 598531. https://doi.org/10.1155/2014/598531.

[23] J. Torres, M. Cole, A. Owji, Z. DeMastry, A.P. Gordon, An approach for mechanical property optimization of fused deposition modeling with polylactic acid via design of experiments, Rapid Prototyp. J. 22 (2016) 387–404. https://doi.org/10.1108/RPJ-07-2014-0083.

[24] J.M. Chacón, M.A. Caminero, E. García-Plaza, P.J. Núñez, Additive manufacturing of PLA structures using fused deposition modelling: Effect of process parameters on mechanical properties and their optimal selection, Mater. Des. 124 (2017) 143–157. https://doi.org/10.1016/j.matdes.2017.03.065.

[25] C. McIlroy, P.D. Olmsted, Disentanglement effects on welding behaviour of polymer melts during the fused-filament-fabrication method for additive manufacturing, Polymer (Guildf). 123 (2017) 376–391. https://doi.org/10.1016/j.polymer.2017.06.051.

[26] J. Allum, A. Gleadall, V. Silberschmidt, Fracture of 3D-printed polymers: crucial role of filament-scale geometric features, Eng. Fract. Mech. 224 (2020) 106818. https://doi.org/10.1016/j.engfracmech.2019.106818.

[27] ASTM International. D1708-18 Standard Test Method for Tensile Properties of Plastics by Use of Microtensile Specimens. West Conshohocken, PA; ASTM International, (2018). doi: https://doi.org/10.1520/D1708-18

[28] A. Moetazedian, A. Gleadall, X. Han, V. V. Silberschmidt, Effect of environment on mechanical properties of 3D printed polylactide for biomedical applications, J. Mech. Behav. Biomed. Mater. 102 (2020) 103510. https://doi.org/10.1016/j.jmbbm.2019.103510.

[29] Y. Bin, B. Yang, H. Wang, The effect of a small amount of modified microfibrillated cellulose and ethylene–glycidyl methacrylate copolymer on the crystallization behaviors and mechanical properties of polylactic acid, Polym. Bull. 75 (2018) 3377–3394. https://doi.org/10.1007/s00289-017-2215-8.

[30] X. Meng, N.A. Nguyen, H. Tekinalp, E. Lara-Curzio, S. Ozcan, Supertough PLA-silane nanohybrids by in situ condensation and grafting, ACS Sustain. Chem. Eng. 6 (2018) 1289–1298. https://doi.org/10.1021/acssuschemeng.7b03650.

[31] C. Zhang, Y. Huang, C. Luo, L. Jiang, Y. Dan, Enhanced ductility of polylactide materials: Reactive blending with pre-hot sheared natural rubber, J. Polym. Res. 20 (2013). https://doi.org/10.1007/s10965-013-0121-9.

[32] T.Y. Qiu, M. Song, L.G. Zhao, Testing, characterization and modelling of mechanical behaviour of poly (lactic-acid) and poly (butylene succinate) blends, Mech. Adv. Mater. Mod. Process. 2 (2016) 0–11. https://doi.org/10.1186/s40759-016-0014-9.

[33] H. Zhang, J. Huang, L. Yang, R. Chen, W. Zou, X. Lin, J. Qu, Preparation, characterization and properties of PLA/TiO2 nanocomposites based on a novel vane extruder, RSC Adv. 5 (2015) 4639–4647. https://doi.org/10.1039/c4ra14538k.

[34] I. Restrepo, N. Benito, C. Medinam, R. V. Mangalaraja, P. Flores, S. Rodriguez-Llamazares, Development and characterization of polyvinyl alcohol stabilized polylactic acid/ZnO nanocomposites, Mater. Res. Express. 4 (2017). https://doi.org/10.1088/2053-1591/aa8b8d.

[35] W. Song, H. Liu, F. Chen, J. Zhang, Effects of ionomer characteristics on reactions and properties of poly(lactic acid) ternary blends prepared by reactive blending, Polymer (Guildf). 53 (2012) 2476–2484. https://doi.org/10.1016/j.polymer.2012.03.050.

[36] M. Ashby, D. Cebon, M.F. Ashby, Materials selection in mechanical design, J. Phys. IV Colloq. 111 (1993) 3. https://doi.org/10.1051/jp4:1993701ï.

[37] F. Knoop, A. Kloke, V. Schoeppner, Quality improvement of FDM parts by parameter optimization, AIP Conf. Proc. 1914 (2017) 190001. https://doi.org/10.1063/1.5016790.

[38] D. Thaler, N. Aliheidari, A. Ameli, Mechanical, electrical, and piezoresistivity behaviors of additively manufactured acrylonitrile butadiene styrene/carbon nanotube nanocomposites, Smart Mater. Struct. 28 (2019) 084004.

https://doi.org/10.1088/1361-665x/ab256e.

[39] M.S. Uddin, M.F.R. Sidek, M.A. Faizal, R. Ghomashchi, A. Pramanik, Evaluating mechanical properties and failure mechanisms of fused deposition modeling acrylonitrile butadiene styrene parts, J. Manuf. Sci. Eng. 139 (2017) 081018. https://doi.org/10.1115/1.4036713.

[40] S. Wacharawichanant, L. Noichin, S. Bannarak, S. Thongyai, Morphology and properties of acrylonitrile-butadiene-styrene/ZnO nanocomposites with compatibilizer, Macromol. Symp. 354 (2015) 163–169. https://doi.org/10.1002/masy.201400111.

[41] L. Behalek, J. Safka, M. Seidl, J. Habr, J. Bobek, Fused deposition modelling vs. Injection moulding: Influence of fiber orientation and layer thickness on the mechanical properties, MM Sci. J. 2018 (2018) 2722–2726. https://doi.org/10.17973/MMSJ.2018_12_2018117.